Fall 2021

GAS PHASE ION/MOLECULE REACTIONS BETWEEN MONOCATIONIC METAL-BIPYRIDYL (METAL = CU, AG, AU) COMPLEXES AND SMALL GAS MOLECULES USING ION TRAP MASS SPECTROMETER

Shan Chen
University of New Hampshire, Durham

GAS PHASE ION/MOLECULE REACTIONS BETWEEN MONOCATIONIC METAL-BIPYRIDYL (METAL = CU, AG, AU) COMPLEXES AND SMALL GAS MOLECULES USING ION TRAP MASS SPECTROMETER

BY

Shan Chen

B.S. in Environmental Science,

China Pharmaceutical University, 2017

THESIS

Submitted to the University of New Hampshire

in Partial Fulfillment, of

the Requirements for the Degree of

Master of Science

in

Chemistry

September 2021

This thesis was examined and approved in partial fulfillment of the requirements for the degree of Master of Science in Chemistry by:

Thesis director, Anyin Li, Assistant Professor of Chemistry

Christopher Bauer, Professor of Chemistry

Gonghu Li, Professor of Chemistry

On May 27, 2021

Table of Contents

Dedication

This thesis is dedicated to my parents, who raised me up, support my study,

and support all my decisions.

To my teachers, who opened me the door to knowledge.

To my friends, who inspired and motivated me.

Acknowledgement

Firstly, I would like to express my gratitude to my advisor Dr. Anyin Li for his advising on the experiments and guidance on my research in UNH. I would also like to thank my committee member, Dr. Gonghu Li, who have ever given me many suggestions and comments on my progress report, proposal etc. I would thank the other committee member Dr. Bauer Christopher, who also joined my proposal defense and proposed many useful questions. Thank Prof. Christine Caputo for attending my progress report and gave many useful suggestions.

I would like to thank Prof. Rudi Seitz, Prof. Sterling Tomellini, Prof. Arthur Greenberg, Prof. Sam Pazini for their amazing classes, I really enjoyed their teaching and learned a lot.

I would thank all members in Li Group, Taoqing Wang, Huishan Li and Nick Allen, for their help and support during my stay in UNH. Thank Dr. Mengtian Li, who ever gave me many suggestions, both on research and in life.

Thank all the faculties and staff in UNH, thank Cindi, Laura, Kristin for their contributions to the department.

I would thank all people I met in UNH.

List of Figures

List of Tables

ABSTRACT

GAS PHASE ION/MOLECULE REACTIONS BETWEEN MONOCATIONIC METAL-BIPYRIDYL (METAL = CU, AG, AU) COMPLEXES AND SMALL GAS MOLECULES USING ION TRAP MASS SPECTROMETER

By

Shan Chen

Ion/molecule reactions happens in the very diluted low-pressure environment provided by mass spectrometer. Studying ion/molecule reactions in gas phase may reveal novel chemistries of the pertinent reactants and products. The convenience of isolating target reactant ions with multistage MS in the gas phase eliminates the involvement of solvent or counterions which could add unnecessary complexity for interpreting novel chemistry. A lot of research has been applied to the metal-bipyridine system in the solution phase, but not too much research reported in the gas phase.

In this work, the study of metal-bipyridine system has been extended to the gas phase with aid of Mass Spectrometer. Monocationic metal-bipyridyl $[M\text{-}bpy]^+$ complexes (Metal = Cu, Ag, Au) were produced in the gas phase with electrospray coupled with MS/MS, reactions with water gas and nitrogen gas were performed inside the Linear Quadrupole Ion Trap, and the full reaction process was detected by Mass Spectrometer synchronously. Product peaks for water adduct ($[H_2OM\text{-}bpy]^+$) and nitrogen adduct ($[N_2M\text{-}bpy]^+$) are observed on the mass spectrum. Kinetic study shows the gas phase reaction follows pseudo-first order with respect to $[M\text{-}bpy]^+$ for Cu and Au. The attributes of products were further investigated with Density Functional Theory (DFT) at

PBE0/cc-pVTZ/cc-pVTZ-PP level, including the geometry optimization and IR prediction. Thermo stability was calculated for the dissociation process. For a given gas, gold complex has the highest binding ability followed by copper and silver complexes. For the dissociation process from the respective bound complexes, they are all indicated as endothermic processes under vacuum and at room temperature. The metal complexes are also found to act as mild bond activation reagents for small gas molecules, with gold complex being the best candidate for O-H activation of water and copper complex being the best for nitrogen bond activation of N_2. Compared with the bond length in free gases, the bond lengths of O-H and N≡N get elongated in the complexes with the optimized structures. In addition, the IR spectra predict a major red-shift in correspond to the stretch frequency of O-H and N≡N in the complexes. Ligands effects are also predicted with calculations, and the results show that phenanthroline perform similar ability binding with water and nitrogen gas molecules as bipyridine.

CHAPTER I: INTRODUCTION

1.1 Introduction of ion/molecule reactions in gas phase

The first ion/molecule reaction with Mass Spectrometry was proposed in 1916 by Dempster[1] who also designed the technique electron ionization (EI). He identified the ions presented the mass to charge ratio 3 is the product for the reactions between H_2^+ and H_2. However, at the beginning of 20th century, mass spectrometrists were mostly focusing on understanding the complexity of the mass spectra so that they largely overlooked the ion/molecule reaction chemistry. It was not until 1966 that Munson and Field[2] discovered that ion/molecule reaction can replace the electron ionization to create a softer ionization method, which is chemical ionization. Chemical ionization often involved proton transfer from charged solvent molecules to the analyte. Thereafter, explosive number of studies on ion/molecule reactions are reported, including functional group identification or isomer identification. With the development of Mass Spectrometry, the mass spectrometer has become an instrumental tool that widely used to study organic chemistry other than analytical chemistry. Ion/molecule reactions also contribute to unravel the reaction mechanisms of organic reactions, helping to bridge the gap between condense-phase organic chemistry and gas-phase ion chemistry. A lot of classical organic reactions have been studied with MS methods. For example, the nucleophilic substitution reaction,[3-5] [4+2] Diels-Alder cycloaddition reaction,[6-7] Michael addition[8] and so on. With the broad use of electrospray, mass spectrometry becomes a versatile tool to study the inorganic and organometallic chemistry,[9-11] because electrospray possesses the advantages that the metal complex can be easily transferred from the solution phase to the gas phase without altering the oxidation state.[12-13]

Compared with reactions in the solution phase, gas phase supplies several unique advantages. Firstly, reactions in the gas phase are efficient, fast, and highly sensitive. They generally take only femtoseconds, and MS can detect the products at trace level.[14-15] For studying the mechanism of organic reactions,[16-17] gas phase can provide the detailed information about single step and allows the study of transient intermediate which has never been accessed through techniques in the solution phase. Moreover, the reaction in the gas phase may provide intrinsic chemical or physical properties of the ions which can be hidden in the solution phase because of the solvent effect or ion-pairing effect.[18-19] In some cases, the performance of ions in gas phase is consistent with the performance in solution phase.[20] However, there is also observation that solvent molecule has significant effect on the performance of ions, affecting the reactivity and energy partitioning. For instance, Mackay[21] and Heril[22] groups worked on the solvent effect of nucleophilic substitution of CH_3Cl and CH_3Br, and they found that the presence of water solvent molecules suppresses the reaction rate coefficient. And they also found that the most abundant product in gas phase was not the thermo favored solvated product ion like in the solution phase, but the free solvated ion. Schettino[23] and Yu[24] group also found that the water solvent molecule can lower the reactivity. With Mass spectrometry, the ability to isolate the specific ions provides flexibility to select the ions with or without solvent molecules.

1.2 Introduction of Linear Quadrupole Ion Trap

Ion trap is a setup to confine ions in a small space by elaborately applying the magnetic field and electric field to the electric charges. Due to the capacity to trap ions provided by the ion trap, W. Paul and H. Steinwedel[25] firstly introduced this ion storage device into the mass spectrometer by coupling it to the ionization techniques (e.g., electrospray ionization). They were also the first to unravel a method to trap a range of masses and to detect the ions in mass spectrometry. The mass

analysis with ion trap contributes to the first stage of the development of ion trap mass spectrometry. Followed by that, during 1960s to 1980s, several peer leaders in Mass Spectrometry including John F. J. Todd, N.R. Whetten, P.H. Dawson etc.[26] created a new scan method that through operating the field of quadrupoles, only one single mass can be stored in the trap at a time. The mass-selective storage, or ion isolation is the second age of ion trap mass spectrometry development. George Stafford and many other researchers such as John E. P. Syka and so on promoted the development of the third stage – mass-selective ejection in late 1980s. They firstly disclose a new scan mode of exciting ions and ejecting to the detector, which is a main scan mode being used till today[27]. The development of ion trap mass spectrometer makes it available to more applications including the structure elucidation, multistage MS analysis, providing high sensitivity and resolution to the sample analysis. In addition, the capacity to store ions and high vacuum chamber makes the ion trap mass spectrometer a good device for chemists to study the reactions in the gas phase.

Figure 1.1[28] shows the configuration of an ion trap mass spectrometer (Linear Trap Quadrupole Mass Spectrometer, or LTQ-MS) with different pressures for each chamber and operational voltages for each part of the device. Analyte ionized in the ionization source with different techniques (Electrospray ionization for example) is pumped into the mass spectrometer, the solvent gets vaporized when passing the heated capillary, the left analyte ions are energized when going through the accelerating electric field and finally arrive the ion trap, being trapped, isolated, or ejected to the detector eventually[29].

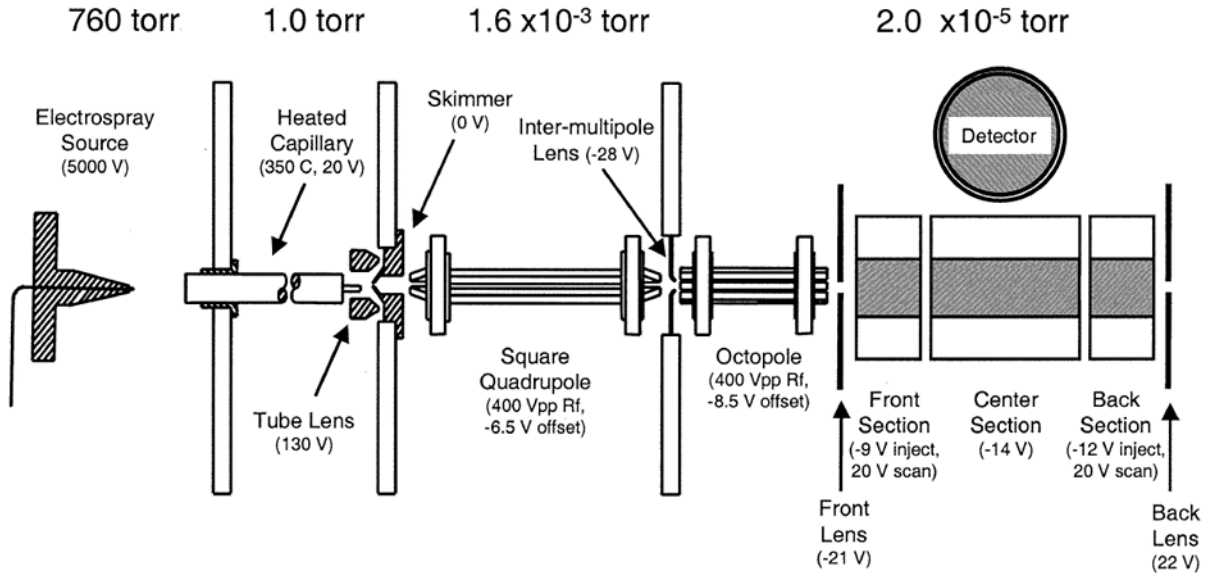

Figure 1.1 Configuration of Linear Trap Quadrupole Mass Spectrometer (LTQ-MS) with operational voltages and pressures. Reprinted with permission from ref 28, Copyright 2002, American Chemical Society.

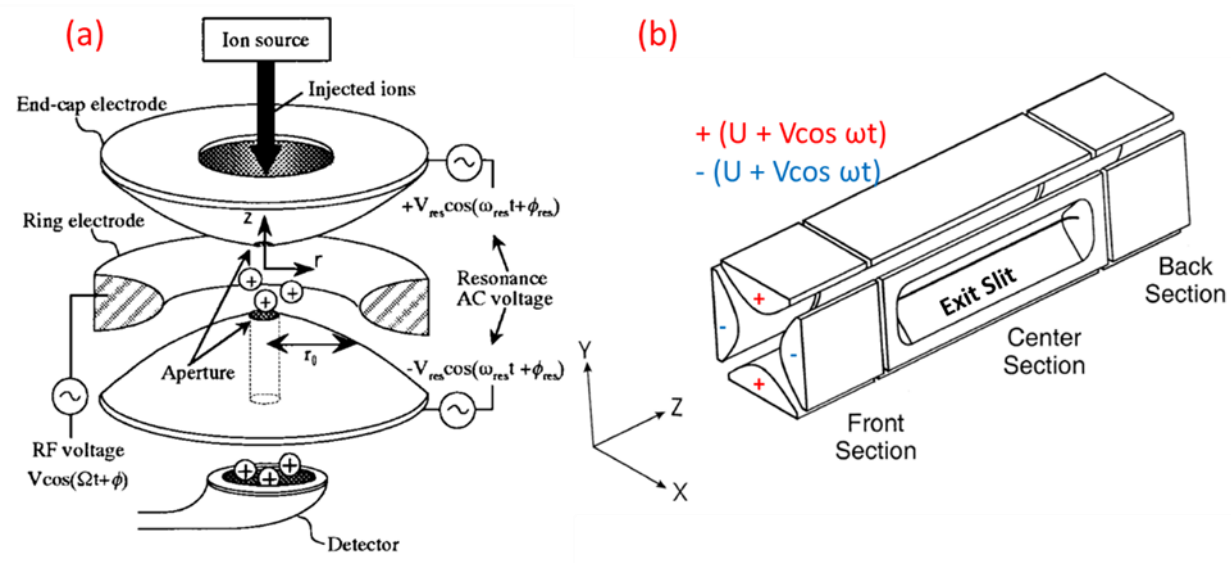

Figure 1.2 Composition of 3D ion trap (left) Reproduced with permission from ref 30. Copyright 2000, Rapid Communication in Mass Spectrometry. Composition of linear quadrupole ion trap (right). Adapted from ref 28. Copyright 2002, American Chemical Society.

The first generation of ion trap used in Mass Spectrometry was developed by W. Paul, which is a 3D ion trap (also called Paul Ion Trap) containing two end caps and one ring electrode (Figure 1.2).[30] In 2002, Jae C. Schwartz and Michael W. Senko[28] in Thermo developed a two-dimensional quadrupole ion trap and demonstrated that it has a better ion capacity, higher sensitivity, and higher resolution than the 3D ion trap. The main configuration of the 2D linear ion trap is made of two pairs of hyperbolic rods with each rod cut into three sections with different lengths (12 mm, 37 mm and 12 mm from the front section to back section). Each rod is applied with both a direct current (DC) voltage as well as an alternating current (AC) voltage with the same polarity on each pair of opposite rods and opposite polarity on each pair of nearby rods (Figure 1.2, right). The ion motion inside an ion trap was well studied and a stability diagram was created by Mathieu (Figure 1.3).[27] The diagram shows the stable and unstable regions for ions using a new set of coordinates *q* and *a*, which are defined as Equation 1-1 and Equation 1-2:

$$q = \frac{4eV}{mr_0{}^2\omega^2} \qquad \text{Equation 1-1}$$

$$a = \frac{8eU}{mr_0{}^2\omega^2} \qquad \text{Equation 1-2}$$

where e is the charge on an ion, V is the zero-to-peak amplitude of the alternating current voltage, m is the mass of ions, r_0 is the radius of the chamber, U is the amplitude of the direct current voltage, and ω is the angular frequency of applied radio frequency (RF) voltage.

Based on the Mathieu Equation and stability diagram, the ions can stay in different status inside the ion trap by adjusting the AC/DC/RF applied on the electrodes.[28] For example, the ions can stay in a stable region thus being trapped in the ion trap in axial direction by applying DC voltages to the electrodes and trapped in radial direction by changing the frequency of AC voltages. The ions

can be excited and fragmented by changing the AC voltages on the electrodes. And ions can be isolated by keeping other ions in the unstable region and leaving targeted ions in the stable region.

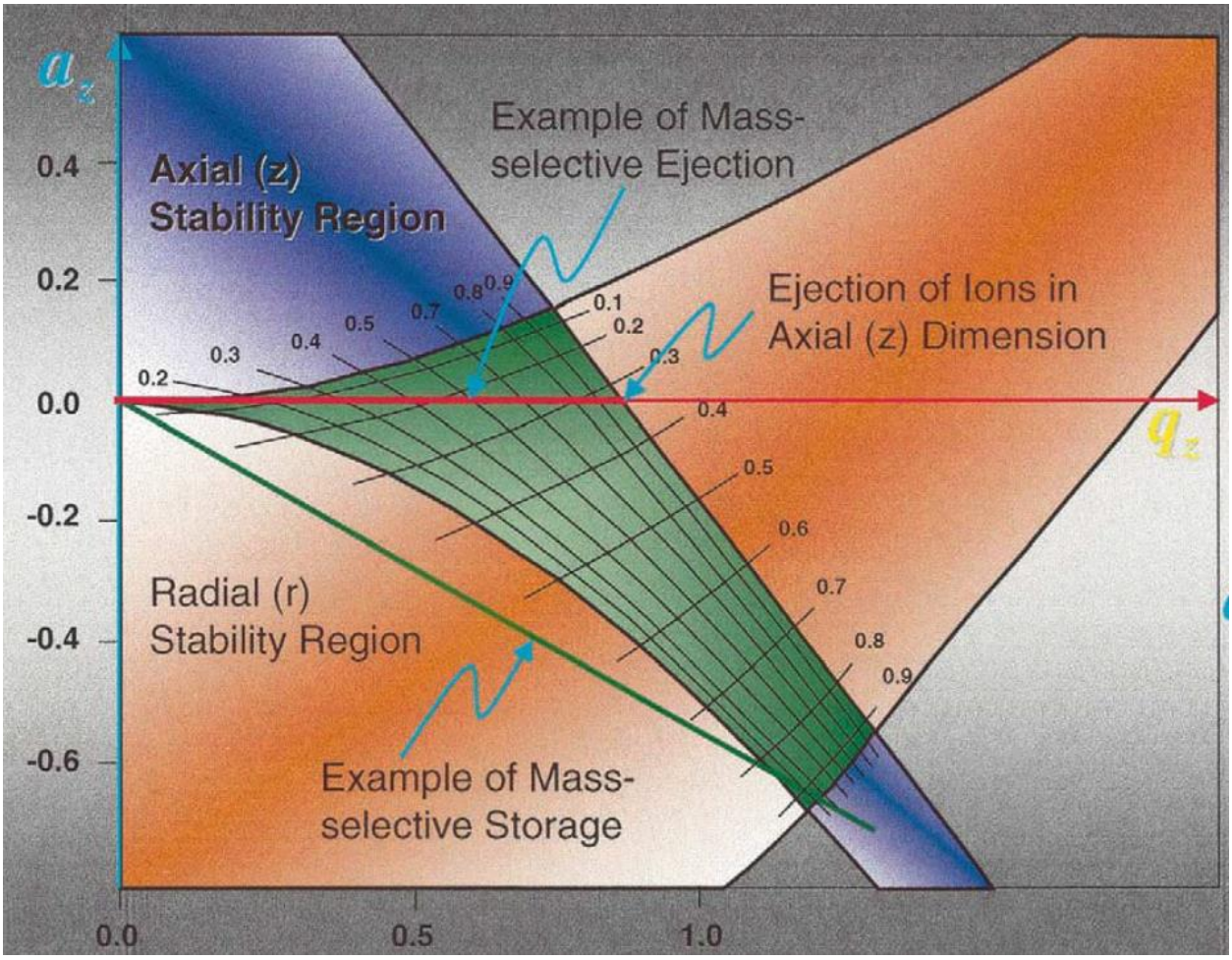

Figure 1.3 Mathieu stable diagram for the ions inside mass spectrometer. Reproduced with permission from ref 27. Copyright 2002, American Chemical Society.

1.3 Synthesis and application of metal-bipyridine complexes (metal = Cu, Ag, Au)

The organometallic chemistry for coinage metal (Cu, Ag, Au) bipyridine [M(bpy)] in the solution phase have been widely studied including the study on theory and study on applications. In around 20th century, researchers mainly work on the fundamental study of complexes, for example, the

interaction of ligands with metal compounds,[31] the crystal morphology,[31-33] the stereometry, and geometry of the complexes with different oxidation states (Figure 1.4).[33] In more recent time, research more focus on the application of complexes including the catalysis and photochemistry. J. M. Mayer group[34] used Cu(II)(bpy) as catalyst for reduction of water, and Orellana group[35] discovered Ag(II)$(bpy)_2$ can be utilized to functionalize the C-H bond directly. Besides, metal-bipyridine complex also have large contribution in the field of sensor[15] or biochemistry[36]. However, the study of [M(bpy)] in the gas phase are not as much as in the solution phase, mainly focusing on the theoretical computation[37] or physical study[38].

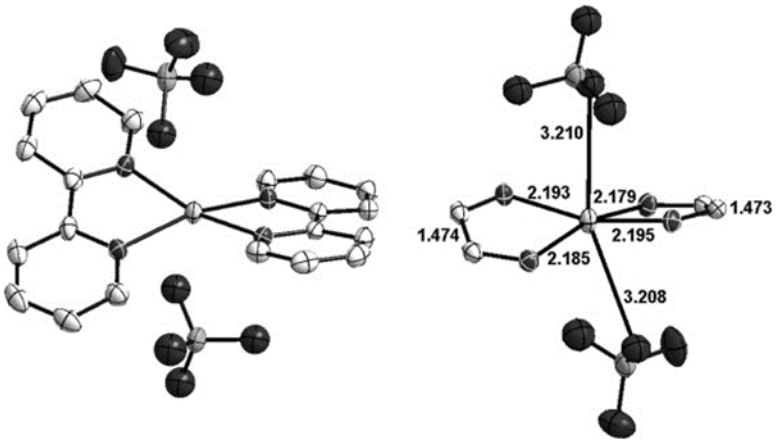

Figure 1.4 $[Ag(bpy)_2]^{2+}$ cation in solid state $[Ag(bpy)_2](ClO_4)_2$ and computation of representative bond lengths. Reproduced with permission from ref 33. Copyright 2012, Polyhedron.

In the solution phase, a lot of methods[31,39-40] have been developed to synthesize the complex, the most common method is mixing the metal salt with ligands, after stirring, evaporation of solvent, the target complex can be roughly synthesized. The products need more operations like recrystallization for get purified. Reactions in solution phase usually take long time (at least 30 min), and large amount of ingredients are necessary. Evaporation of solvent creates a waste of solvent and increases the expense, and recrystallization makes the process complicated to get pure

products. However, R. G. Cooks group[41] discovered that metal could get oxidized gradually with electrospray under high voltage, by adding the ligands into the solution, the complex will form during the electrospray process. To make different kinds of complexes, metal can be changed through changing the electrode, and ligand can be changed by changing the solutions. Most kinds of complexes can be synthesized through electrospray[38]. The formation of complex only takes a few minutes, which greatly saves the time. Besides, the concentration of ligands is under part-per-million (ppm) level in most circumstances, and the volume is under 100 μL, which saves a lot of chemicals and solvents.

In this research, the monocationic coinage metal complexes in gas phase are formed through electrospray, tandem MS is coupled to remove extra ligands. Bipyridine is selected as the ligand due to the relative simplicity and the ability to interact with many different metals. The single charged metal-bipyridine complex $[M(bpy)]^+$ (M= Cu, Ag, Au) will further react with small gas molecules (e.g. water gas, nitrogen gas) in the ion trap mass spectrometer. Kinetics of the reaction is studied here. Density Functional Theory (DFT) is applied to predict the geometry of complexes and the Thermodynamics of reactions. IR spectra of products and effects of other ligands are also predicted with calculation.

CHAPTER II: EXPERIMENTAL METHODS

2.1 Materials and instruments

2.1.1 Chemicals and materials

All metal electrodes in this research are commercially available, Copper electrode (diameter is 0.3 mm) is from an unknown vender. Silver electrode (99.99+%, 0.25 mm diameter) is bought from Sigma Aldrich (MO, USA). Gold electrode (Premion, 99.998%, 0.1 mm diameter) is purchased from Alfa Aesar (MA, USA). Acetonitrile (ACN) is Certified ACS grade purchased from Fisher Chemical (NJ, USA), 2,2'-Dipyridyl (99+%) is purchased from ACROS ORGANICS (NJ, USA). Borosilicate glass capillaries without filament, (B 150-86-10, o.d., 1.5 mm; i.d., 0.86 mm; 10 cm length) is purchased from Sutter Instrument (CA, USA).

2.1.2 Instruments

Micropipette puller (model P-1000, Sutter Instrument, CA, USA) is used to pull capillary pipette. To get a 3 μm capillary tip, parameters used for puller are listed: Heat is 300 unit, velocity is 17 unit, pressure is 590 unit, and 50 ms cooling time between each trial. Jaw temperature is 21°C.

LTQ-XL Linear trap mass spectrometer is purchased from Thermo Scientific (San Jose, CA, USA). The inlet temperature is 125 °C, inlet capillary voltage is 41 V, Len 0 and Len 1 voltages are -5 V, -38 V, respectively. Front lens voltage is -6.25 V, Gate Len voltage is -76 V. Multipole RF Amplitude voltage is 400 V from peak to peak.

2.2 Synthesis of $[M(bpy)]^+$ complex

Figure 2.1 shows the setup for synthesizing the complexes. Under ambient pressure, the commercially available metal electrode is inserted into a pulled capillary (tip diameter is about 3 μm) filled with 10 μL of bipyridine (1 ppm dissolved in acetonitrile). A high voltage about 1.5 kV

is applied to the electrode. The metals gradually get oxidized when high voltage turns on, complex ions are formed in the solution phase and gradually getting nebulized under the electrical field. An aerosol containing complex ions then get introduced to the mass spectrometer through the inlet. The ions are accelerated and guided to the ion trap with the octupole ion guide. The process is fully monitored with mass spectrometry and several different metal complexes formed during the electrochemical process are observed under full scan. To get the target complex $[M(bpy)]^+$, the precursor ions are selected, with the help of tandem MS, the extra ligands will be removed through collision with Helium gas, the process is called collision introduced dissociation (CID). LTQ tune software is used to control the CID conditions, the isolation window is set as 1.5 Th, and the collision energy is 15% arbitrary unit, q value is 0.30.

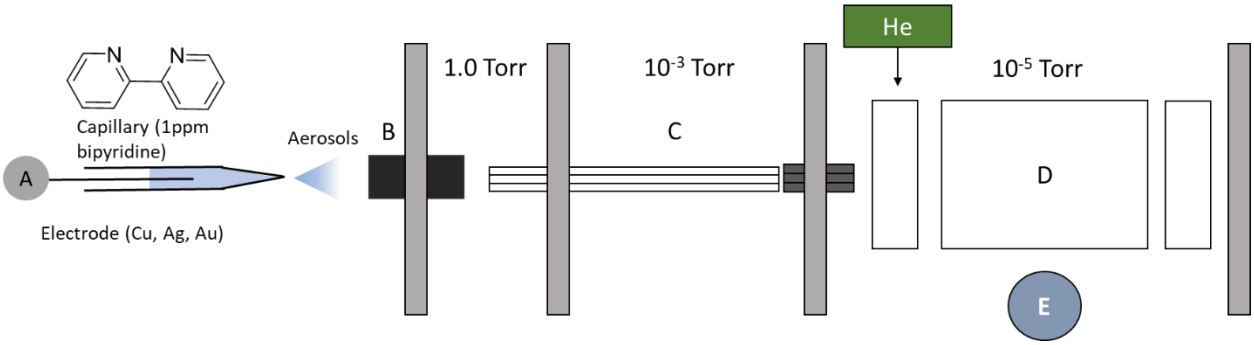

Figure 2.1 Experimental setup to produced complexes in the gas phase with operational pressures. Key components are labeled. The labeled components are listed: A. high voltage supplier, B. inlet, C. octupole ion guides, D. linear ion trap, E. detector, He. Helium gas cylinder. Voltage is 2.0 kV, bipyridine solution is 1 ppm, 10 µL. Auto Gain Control (AGC) is 3E4 for full MS.

2.3 Reaction of $[M(bpy)]^+$ with N_2 and H_2O in Mass Spectrometer

The $[M(bpy)]^+$ ions are formed through tandem MS, then they are isolated with a MS^3 without any activation energy applied, isolation window is 1.5 Th, q value is 0.30. Reaction time is manually controlled by adjusting the "activation time" on the LTQ tune panel. For different metal complexes, different reaction time are applied based on the results of pre-experiments. For copper complex,

reaction time ranges from 10 to 300 ms, for silver complexes, the time is from 30 to 1500 ms, and for gold complex, the reaction time is 10 to 150 ms. No N_2 or H_2O gas needs further introduced to the mass spectrometer because there are already some amounts of gases inside mass spectrometer with a pressure at ca. $1.0 * 10^{-5}$ Torr. Temperature for the reaction is room temperature. Mass spectrum starts to collect under different reaction times when the intensity of $[M(bpy)]^+$ stabilizes. For each spectrum, it is presented with an average of 50 times scan. Thermo Xcalibur Qual Browser (4.0.27.10) is used to collect, process data, and read information needed.

Normalized intensity[42] is calculated as the absolute intensity of individual peak divided by the total intensity of peaks, where the total intensity of peaks means the summary of intensity of bare metal complex $[M(bpy)]^+$, intensity of water addicted peak $[H_2OM(bpy)]^+$ and the intensity of nitrogen addicted peak $[N_2M(bpy)]^+$. To study the reaction order, linear regression for natural logarithm of the normalized intensity of $[M(bpy)]^+$ versus reaction time is plotted for the first order, and linear regression using the reciprocal of normalized intensity of $[M(bpy)]^+$ vs. reaction time is plotted for second order, respectively.[43]

2.4 Computational methods

Density Functional Theory (DFT) calculations were performed to study the ion/molecule reaction. All calculations are calculated with PBE0 functions,[45] the cc-pVTZ basis set is applied to the atoms C, N, O, H and cc-pVTZ-PP with effective core potential (ECP) is applied to the heavy metals Au, Ag and Cu.[44] And the calculations are performed with Gaussian 09W package of programs. GaussView 5.0 software is used to create the model and visualize the results.

Geometry optimization shows the prediction of complex structures and how they interact with gas molecules. Thermostability for all metal complexes is predicted with following aspects:

Bond dissociation energy (BDE), which is calculated as:

$$BDE = \boldsymbol{E}([M(bpy)]^+) + \boldsymbol{E}(L) - \boldsymbol{E}([LM(bpy)]^+) \quad \text{Equation 2-1}$$

Enthalpy change for the dissociation reaction, which is calculated as:

$$\boldsymbol{\Delta H} = \boldsymbol{H}([M(bpy)]^+) + \boldsymbol{H}(L) - \boldsymbol{H}([LM(bpy)]^+) \quad \text{Equation 2-2}$$

Free Gibbs Energy for the dissociation process, which is calculated as:

$$\boldsymbol{\Delta G} = \boldsymbol{G}([M(bpy)]^+) + \boldsymbol{G}(L) - \boldsymbol{G}([LM(bpy)]^+) \quad \text{Equation 2-3}$$

where L represents the small molecules (N_2 or H_2O), which can be recognized as a new ligand to the metal complexes. ***E*** is the "Sum of electronic and thermal energies", ***H*** is the "Sum of electronic and thermal enthalpies", ***G*** is the "Sum of electronic and thermal free energies", that are listed in the output file of Gaussian.

To better explain the interaction between metal complex and gas molecules, orbitals of complexes showed, the orbital are visualized with GaussView with isovalue 0.2. IR is also predicted to study the bonds activation within water and nitrogen. For prediction of the effect of Phenanthroline ligand, all calculations follow the same functions and basis sets as the Bipyridine ligand, and all energy are calculated using the equations stated above.

CHAPTER III: RESULTS AND DISCUSSIONS

3.1 Synthesis of $[M(bpy)]^+$ complexes

3.1.1 Synthesis of $[Cu(bpy)]^+$

The synthesis process is fully monitored by Mass Spectrometer. The Extracted Ion Current (EIC) shows the relative strength of the signals for each peak with time in Figure 3.1 (a) – (c). And the time starts to count when the high voltage turns on. The signal of $[Cu(bpy)_2]^+$ appears firstly and reaches a peak at ca. 3.5 min and decreases subsequently and disappears at ca. 10 min. The signal of $[ACNCu(bpy)]^+$ appears at almost the same as $[Cu(bpy)_2]^+$, but the intensity increases slower than $[Cu(bpy)_2]^+$, the signal keeps at a relative stable level for about 5 min and decreases in the end. The signal for $[Cu(ACN)_2]^+$ also comes out nearly the same time, but a little slower than the other two. The intensity keeps stable increase during the whole process and becomes the dominant peak at last. Figure 3.1 (e) – (f) show several mass spectra presented at specific time points (3.0 min, 6.0 min, 10.0 min) which also shows the tendency of the change of each peak. As time goes, the intensity of $[Cu(bpy)_2]^+$ (m/z 375/377) decreases, followed by $[ACNCu(bpy)]^+$ (m/z 260/262). However, the intensity of $[Cu(ACN)_2]^+$ (m/z 145/147) keeps increasing all the way. The isotopic peaks are caused by the isotopes of copper (^{63}Cu and ^{65}Cu), the ratio of the isotopic peaks is consistent to the ratio of copper which is 2:1, which helps identify that the peaks belong to the copper complexes. The mechanism of this process can be rationalized. Cu is gradually oxidized to Cu^+ under high voltage. And Cu^+ are primarily build connection with two bipyridines to form $[Cu(bpy)_2]^+$ when there is high concentration of bipyridine around. This may because bipyridine is more basic than acetonitrile and bipyridine is a bidentate ligand while acetonitrile is a single dentate ligand. After the bipyridine is largely consumed, there is not enough bipyridine to support

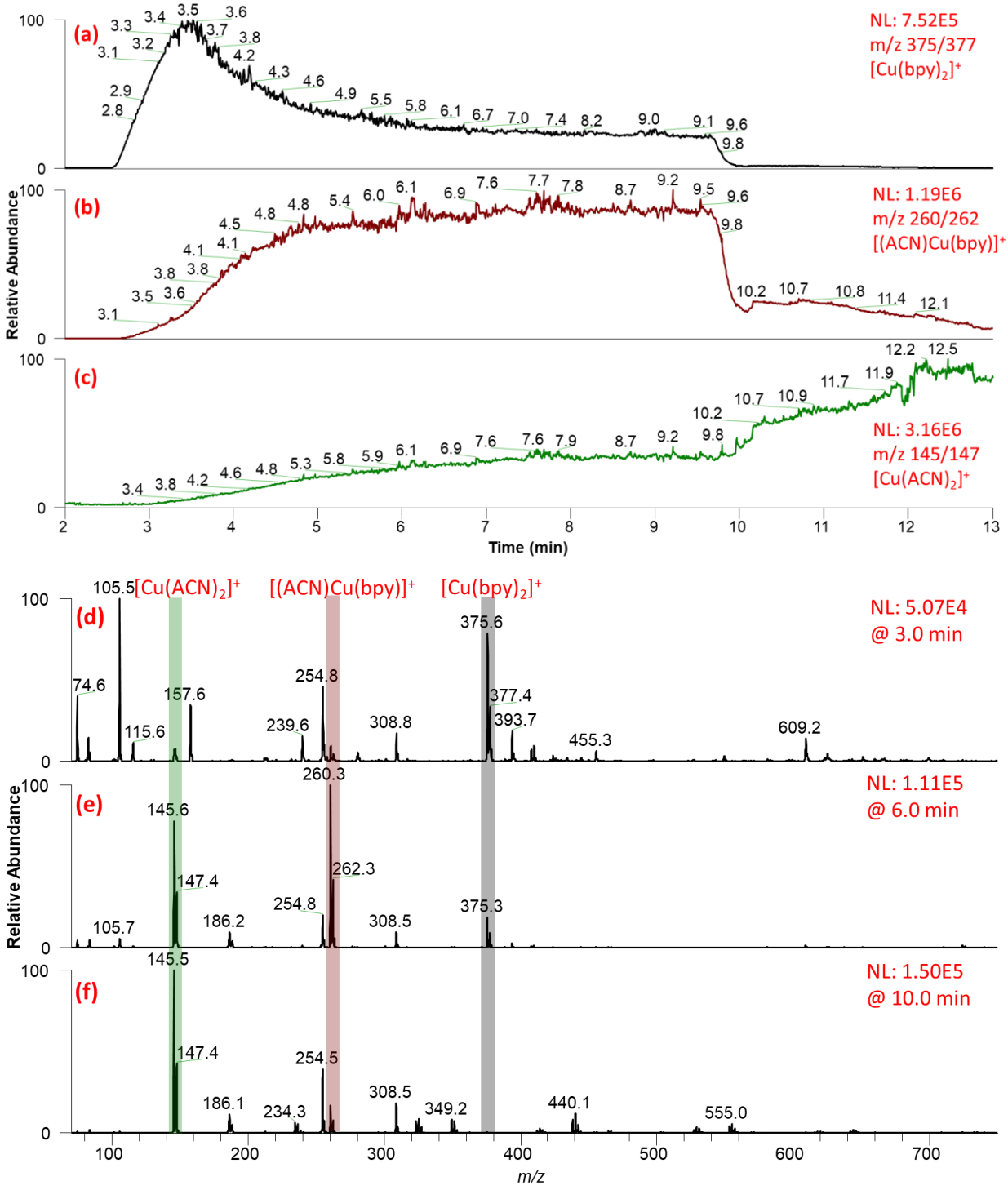

Figure 3.1 Step 1 of synthesis process of $[Cu(bpy)]^+$, (a) – (c) are Extracted Ion Chromatogram for $[Cu(bpy)_2]^+$, $[ACNCu(bpy)]^+$ and $[Cu(ACN)_2]^+$, respectively. (e)-(f) are representative mass spectra at 3.0 min, 6.0 min and 10.0 min, respectively.

the formation of $[Cu(bpy)_2]^+$, resulting in a decrease signal of $[Cu(bpy)_2]^+$. Instead, an alternative $[ACNCu(bpy)]^+$ is preferred because it is more stable than $[Cu(bpy)_2]^+$, so copper is preferring to bind with one bipyridine plus an acetonitrile. After most of the bipyridine get consumed, Cu^+ can only bind with acetonitrile, that is why there is only high intensity of $[Cu(ACN)_2]^+$ in the end.

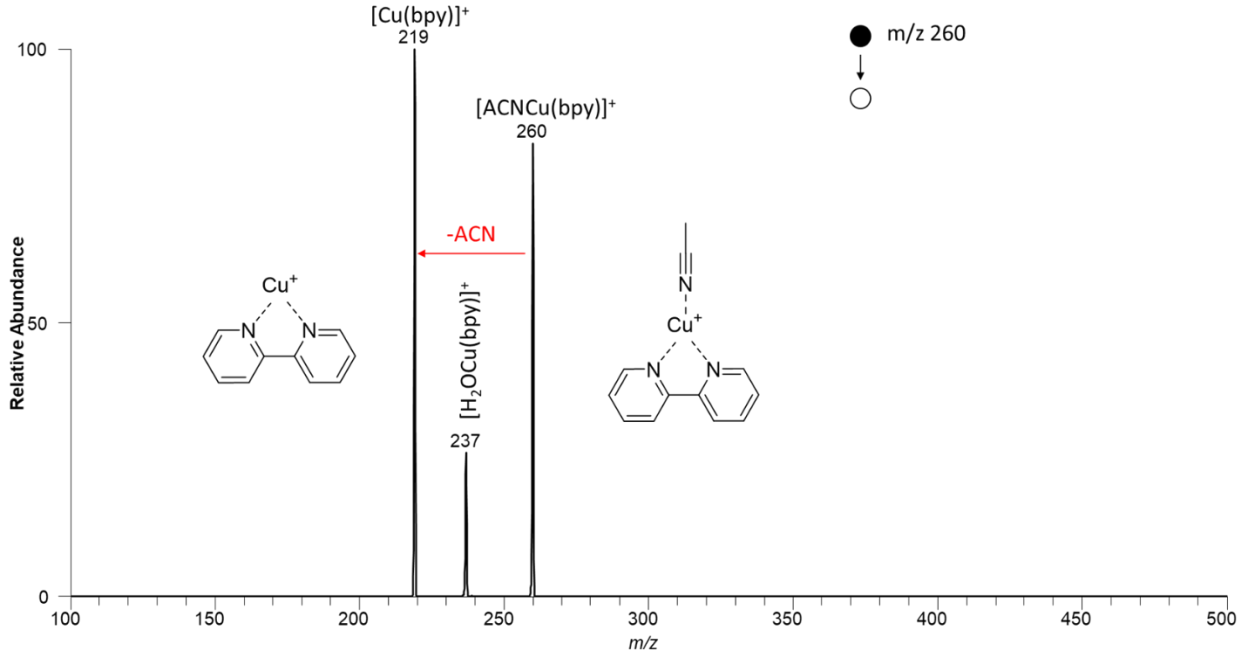

Figure 3.2 Step 2 of synthesis of $[Cu(bpy)]^+$. Tandem MS spectrum of $[(ACN)Cu(bpy)]^+$. Isolation window is 1.5 Th, activation energy is 15%.

To get the $[Cu(bpy)]^+$, either $[Cu(bpy)_2]^+$ or $[(ACN)Cu(bpy)]^+$ can be selected as the precursor ion. With the help of tandem MS, an extra bipyridine or ACN ligand will be removed through the collision with He gas. However, EIC figures show that $[(ACN)Cu(bpy)]^+$ can keep at a stable level with high intensity for a longer time. In order to decrease the influence caused by the fluctuation of ion source, $[Cu(bpy)]^+$ formed from $[(ACN)Cu(bpy)]^+$ are used for the further study.

3.1.2 Synthesis of $[Ag(bpy)]^+$

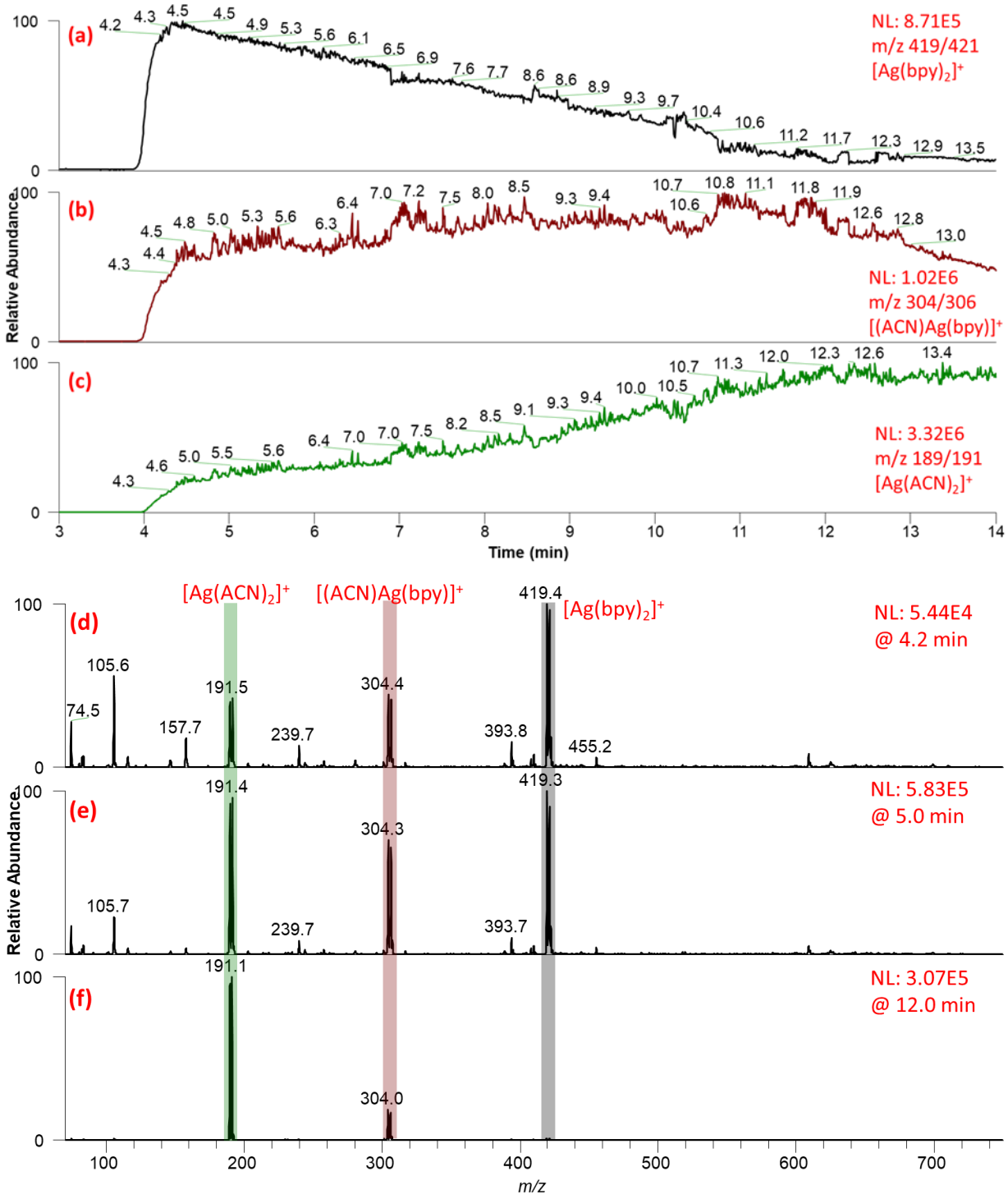

Figure 3.3 Step 1 of synthesis process of $[Ag(bpy)]^+$, (a) – (c) are Extracted Ion Chromatogram for $[Ag(bpy)_2]^+$, $[ACNAg(bpy)]^+$ and $[Ag(ACN)_2]^+$, respectively. (e)-(f) are representative mass spectra at 4.2 min, 5.0 min and 12.0 min, respectively. Voltage is 2.0 kV, bipyridine solution is 1 ppm, 10 µL.

The process to make $[Ag(bpy)]^+$ is quite similar to $[Cu(bpy)]^+$. The EIC curves (Figure 3.2 (a) – (c)) show that the signal of $[Ag(bpy)_2]^+$ appears at ca. 4 min and decreases continuously after it quickly reaches a peak. The signal of $[ACNAg(bpy)]^+$ appears nearly the same time and keeps at a relative stable level from 4.5 min to 12 min. The signal of $[Ag(ACN)_2]^+$ increases during the whole process and becomes the main peak finally. The mass spectra at 4.2 min, 5.0 min and 16.0 min are showed on Figure 3.2 (e) – (f), the 1:1 isotopic peak caused by the 1:1 ratio of ^{107}Ag and ^{109}Ag helps verify the peaks are silver complexes. At the beginning, $[Ag(bpy)_2]^+$ (m/z 419/421) is the highest peak, and then the intensity for $[ACNAg(bpy)]^+$ (m/z 304/306) and $[Ag(ACN)2]^+$ (m/z 189/191) increases and $[Ag(ACN)2]^+$ becomes the main peak in the last which match the change of EIC curves. The reasons to explain this kind of tendency are the same as the formation of copper complexes. $[ACNAg(bpy)]^+$ is used as the precursor ion to produce $[Ag(bpy)]^+$ through MS^2 (Figure 3.4) for further study because of the stability and high intensity of $[ACNAg(bpy)]^+$.

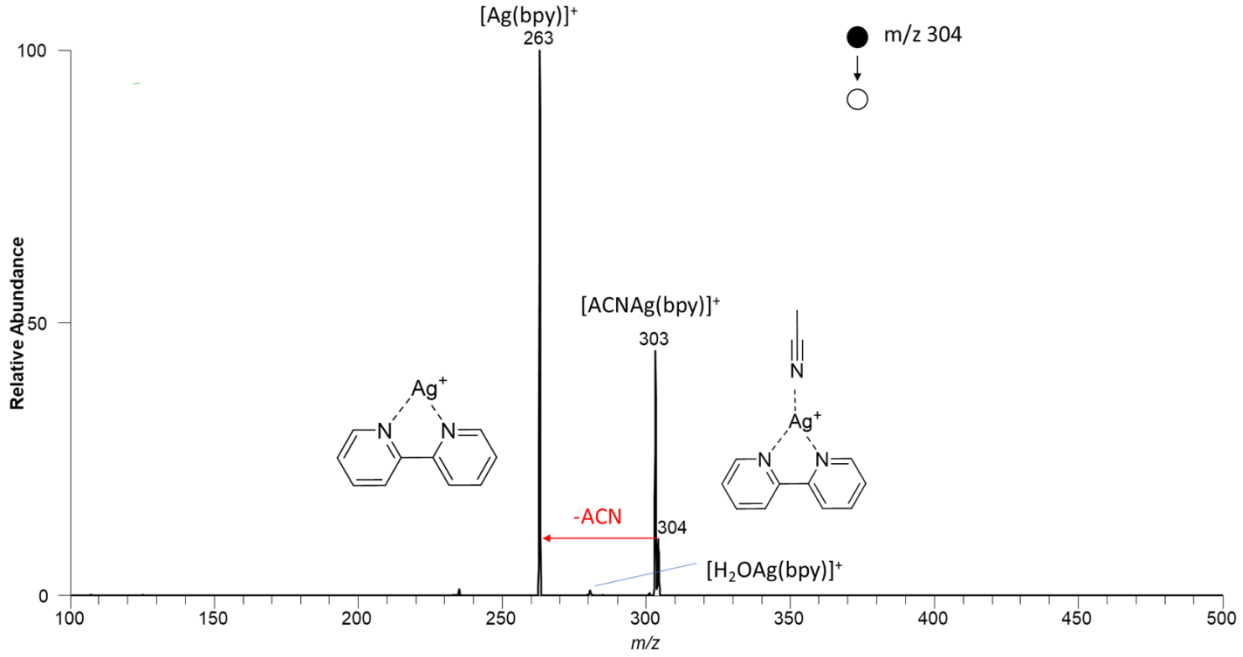

Figure 3.4 Step 2 of synthesis of $[Ag(bpy)]^+$, tandem MS spectrum of $[(ACN)Ag(bpy)]^+$. Isolation window is 1.5 Th, activation energy is 15%.

3.1.3 Synthesis of $[Au(bpy)]^+$

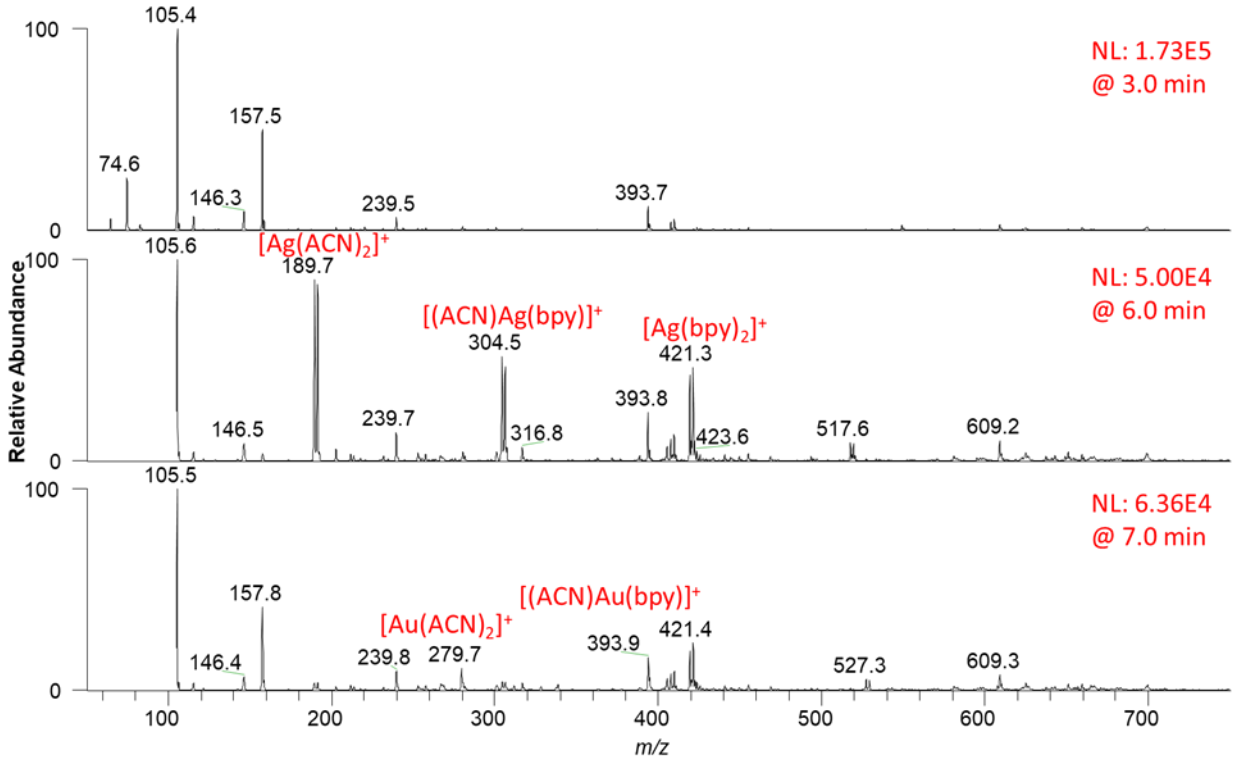

Figure 3.5 Step 1 of synthesis $[Au(bpy)]^+$, full scan of spraying bipyridine with Au electrode at 3.0 min, 6.0 min and 7.0 min, respectively. Voltage is 2.0 kV, bipyridine solution is 1 ppm, 10 µL.

Most part of the process to make $[Au(bpy)]^+$ is similar to the process of copper and silver but there are some differences between them. First difference is that the peak of one of the target ion $[ACNAu(bpy)]^+$ (m/z 394) which is further used to make the $[Au(bpy)]^+$ ion overlaps with a background peak (m/z 394), making it hard to monitor the process to know when the ions will form from EIC curve because there is always a signal for m/z 394 (Appendix A). Besides checking the MS^2 spectrum of the peak to distinguish the ion peak from the background peak (Appendix B), several methods can help estimate when the gold ions formed. Figure 3.5 shows that during the spray, there is a mount of silver complexes formed indicated by the 1:1 ratio peaks and m/z ratio, this is a normal phenomenon because silver is a common impurity during the manufacture of gold

wire and it will be etched out ahead of gold because silver is more active than gold. The appearance of silver complex demonstrates the gold complexes will reach the detector in about 1-2 min based on the evidence of the pre-experiment (Appendix C). A more convenient method is that from the EIC curve of copper and silver, it shows that all of the complexes come out almost at the same time, which support the method that the time can be estimated through appearance of $[Au(ACN)_2]^+$ (m/z 279). These two methods can help to estimate when the needed complex ion will be made, and further reactions can be performed. The other difference is that, compared with copper and silver complexes, there is no peak for $[Au(bpy)_2]^+$ (m/z 505), which may because the high concentration of bipyridine is consumed by Ag^+ to form $[Ag(bpy)_2]^+$ and there is not enough high concentration of bipyridine left to support the formation of $[Au(bpy)_2]^+$. The other hypothesis is that the size of gold is larger than copper and silver, so the orbitals of gold ion may not overlap well with the orbitals of two bipyridines at the same time to make a stable complex $[Au(bpy)_2]^+$.

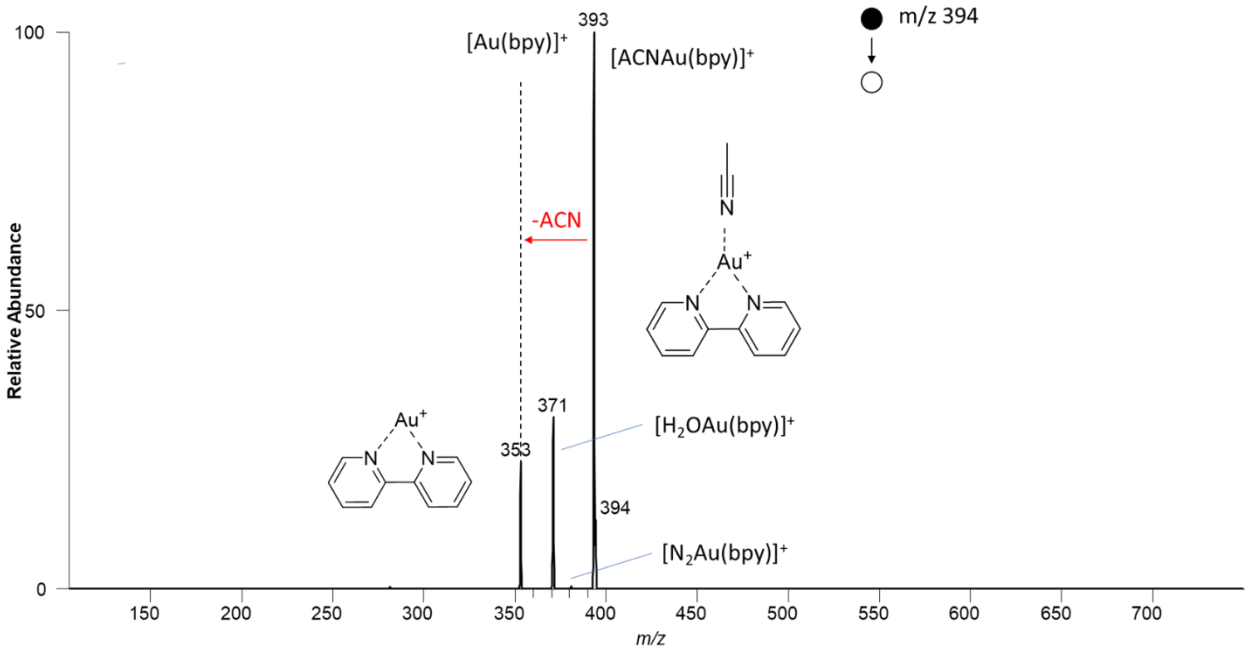

Figure 3.6 Step 2 of synthesis of $[Au(bpy)]^+$, tandem MS spectrum of $[ACNAu(bpy)]^+$. Isolation window is 1.5 Th, activation energy is 15%.

To get $[Au(bpy)]^+$, $[ACNAu(bpy)]^+$ is isolated, and ACN ligand is removed through collision with He gas (Figure 3.6).

3.2 Kinetic study of $[M(bpy)]^+$ with small gas molecules

3.2.1 $[Cu(bpy)]^+$

In figure 3.7 (a), the mass spectrum represents the peaks for both the reactant $[Cu(bpy)]^+$ (m/z 219), water adduct $[H_2OCu(bpy)]^+$ (m/z 237) and nitrogen adduct $[N_2Cu(bpy)]^+$ (m/z 247) where a 50 times magnification is applied for the nitrogen adduct after 100 ms reaction. Plots containing the constitution of the reactants and products are showed in Figure 3.7 (b) and (c). The normalized intensity is calculated as the absolute intensity of each peak divided by the total intensity where the total intensity means the summary of the intensity of all complexes. When the reaction increases in time, more of the reactants are converting to the products. The reacts goes pretty fast, nearly 20% of $[Cu(bpy)]^+$ is consumed only for 10 ms reaction. Over 300 ms, 90% of $[Cubpy]^+$ are reacted to form the water adduct $[H_2OCu(bpy)]^+$. Besides water adduct, there is also a small amount (0.1% - 0.2%) of nitrogen adduct observed for first 150 ms (Figure 3.7 (c)), which means this copper complex can also bind with nitrogen gas. But the water product is more favorable, mainly because $[Cu(bpy)]^+$ is more likely to form connection with water and the water product is more stable than nitrogen.

The natural logarithm of the normalized intensity of reactant $[Cu(bpy)]^+$ and reciprocal of the normalized intensity of $[Cu(bpy)]^+$ against reaction time are showed in Figure 3.7 (d) and (e). The linear relationship between ln $[Cu(bpy)]^+$ vs. time indicates that the reaction performs the first order with respect to $[Cu(bpy)]^+$. The rate constant is 0.0081 ms^{-1}. First order reaction means the H_2O or N_2 will not affect the reaction rate. In this case, it is because H_2O or N_2 are in an excess

amount and the amount stay constant during the reaction. And therefore, it is preferred to call this reaction follows pseudo-first order reaction[46] with respect to $[Cu(bpy)]^+$.

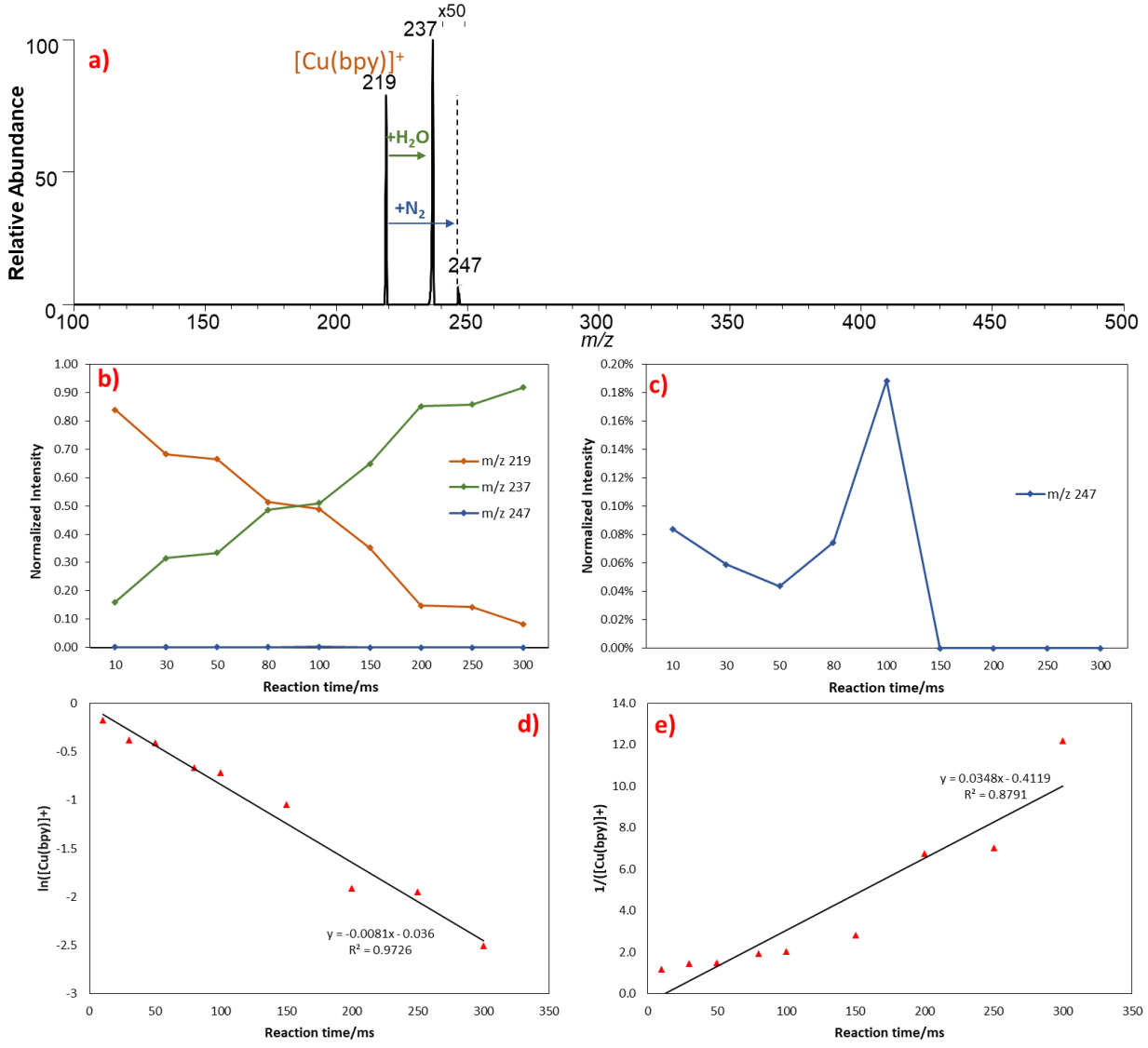

Figure 3.7 (a) Representative mass spectrum showing the reactants and products of the reactions after reacting for 100 ms, 50 scans are averaged. (b) The ratio change of each component with different reaction times. (c) Zoom in curve for m/z 247 in Figure (b). (d) 1st order regression with respect to $[Cu(bpy)]^+$. (e) 2nd order regression with respect to $[Cu(bpy)]^+$.

3.2.2 $[Ag(bpy)]^+$

Figure 3.8 (a) shows the spectrum of the reaction of $[Ag(bpy)]^+$ with neutral gas molecules. m/z 263 corresponds to $[Ag(bpy)]^+$, theoretical m/z of water adduct is m/z 281, but m/z 280 is observed here, this peak is still correspond to the water adduct based on CID spectrum of m/z 280 (Appendix D), it is may because there is a slightly mass shift in this region of the instrument. Theoretical m/z of nitrogen adduct is m/z 291, but no peak observed in the range m/z 285 to m/z 300, even with a magnification of 50 times for the peak intensity. Compared with $[Cu(bpy)]^+$, there is more reactants and less products observed. As the reaction goes for 1500 ms, there is still about 94% of the reactants remained (Figure 3.8 (b)) and only 6% of water product being observed (Figure 3.8 (c)). And during the reaction time from 30 second to 100 second and after 800 second, the intensity of $[Ag(bpy)]^+$ does not change too much. This may relate to the source that provides the target metal complex. Different from the reactions in the solution phase, the initial concentration of the reactants will not change during the reaction. However, in this research, $[Ag(bpy)]^+$ is made from $[ACNAg(bpy)]^+$, the production of $[ACNAg(bpy)]^+$ is an endless process as long as the high voltage is applied on and the solution in capillary does not run out. Therefore, there is continuous production of $[Ag(bpy)]^+$ at the same time when reacting with gas molecules. At the first 100 ms seconds, the consumption rate of $[Ag(bpy)]^+$ may equal or less than the production rate, which creates an equilibrium with respect of $[Ag(bpy)]^+$, therefore, at the beginning, the normalized intensity of $[Ag(bpy)]^+$ in the gas phase keeps at a relative stable ratio. And the intensity of $[Ag(bpy)]^+$ slightly decreases between 100 ms to 800 ms. After 800 ms, the intensity stables again, which mainly because that the water adduct is not stable in the gas phase, when the reaction goes for longer time, $[H_2OAg(bpy)]^+$ may break up to form $[Ag(bpy)]^+$ again which create another equilibrium for longer reaction time. This problem was not observed in the copper complex mainly

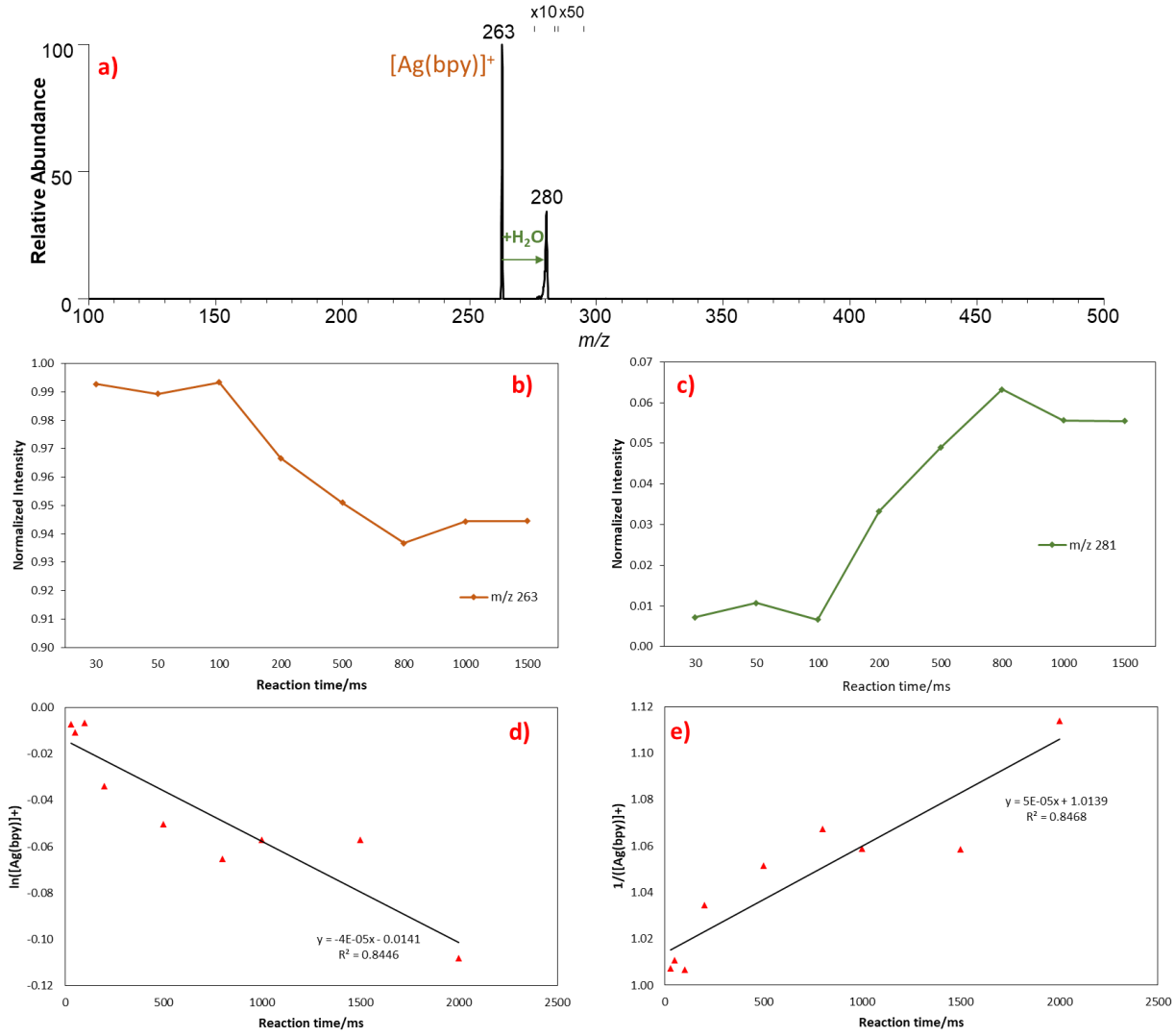

Figure 3.8 (a) Representative mass spectrum showing reactants and products after reaction goes 100 ms, 50 scans are averaged. (b) The ratio change of reactant at different reaction times. (c) The ratio change of water adduct at different reaction times. (d) 1st order regression with respect to $[Ag(bpy)]^+$. (e) 2nd order regression with respect to $[Ag(bpy)]^+$.

because the reaction rate of $[Cu(bpy)]^+$ is fast enough and the products of copper are stable so that the fluctuations can be ignored. With the normalized intensity, reaction order does not show a higher relativity for either 1st order reaction or 2nd order reaction (Figure 3.8 (d) and (e)). But it is

highly believed it follows a pseudo-first order reaction with respect to $[Ag(bpy)]^+$ because this reaction process is similar to the reaction of $[Cu(bpy)]^+$.

3.2.3 $[Au(bpy)]^+$

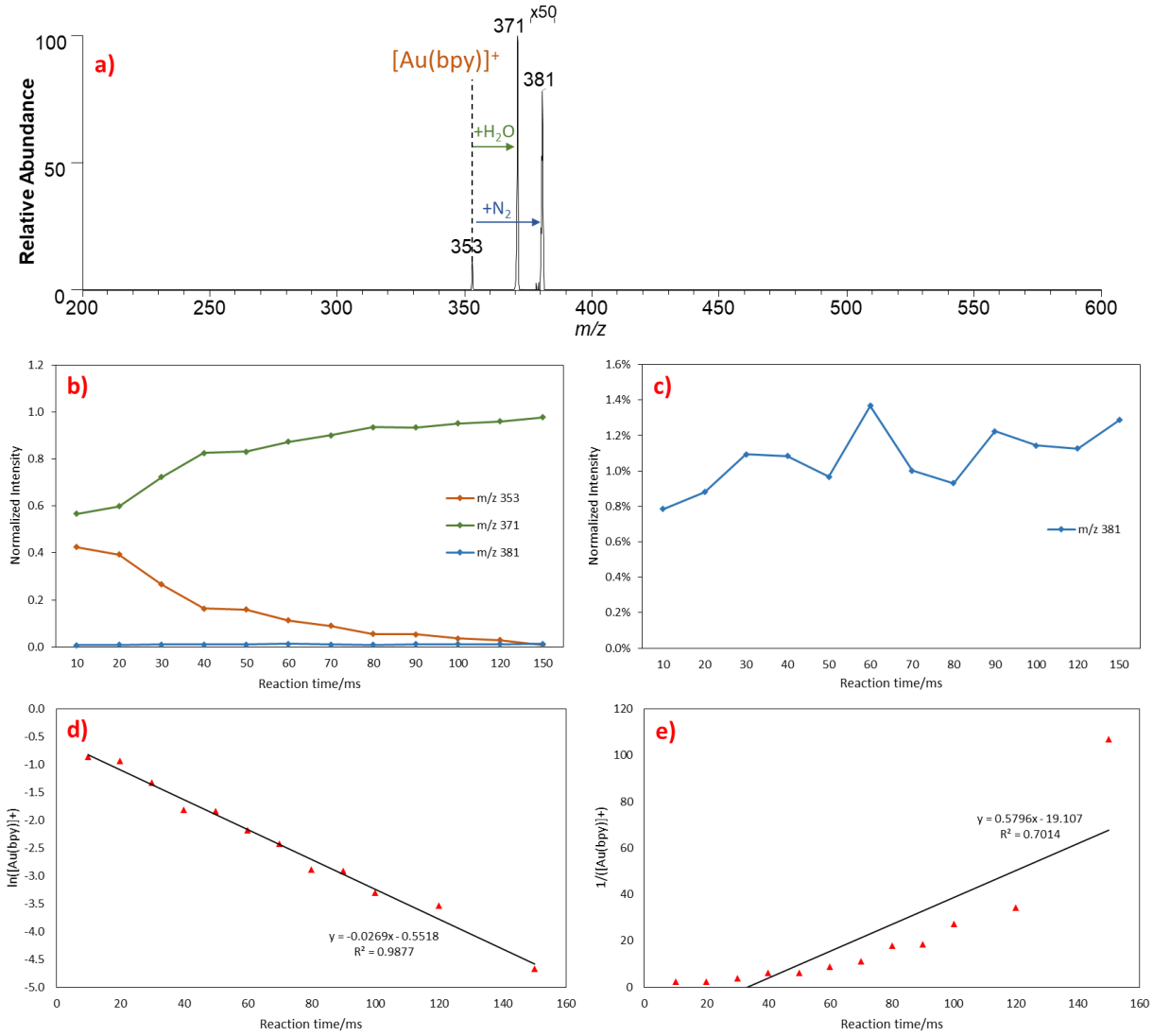

Figure 3.9 (a) Representative mass spectrum of products of the reactions after 100 ms reaction, 50 scans are averaged. (b) The ratio change of reactants and products at different reaction time. (c) zoom in curve for m/z 381 in Figure (b). (d) 1st order regression with respect to $[Au(bpy)]^+$. (e) 2nd order regression with respect to $[Au(bpy)]^+$.

The representative mass spectrum for reaction between $[Au(bpy)]^+$ and gas molecules is showed in Figure 3.9 (a). The peaks from left to right corresponds to $[Au(bpy)]^+$ (m/z 353), the water adduct $[H_2OAu(bpy)]^+$ (m/z 371) and nitrogen product $[N_2Au(bpy)]^+$ (m/z 381), respectively. And Figure 3.9 (b) shows the normalized intensity of each component with different reaction time. Compared with $[Cu(bpy)]^+$, $[Au(bpy)]^+$ is a more reactive reactant with 60% of $[Au(bpy)]^+$ getting reacted in 10 ms, and nearly all $[Au(bpy)]^+$ getting reacted in 150 ms. Moreover, there is also a larger portion of the nitrogen adduct of ca. 1.1% (Figure 3.9 (c)) compared with $[Cu(bpy)]^+$, which means $[Au(bpy)]^+$ works better on binding with nitrogen gas and the nitrogen product is more stable. By comparing the regression of reaction order, the reaction also follows a pseudo-first-order with respect to $[Au(bpy)]^+$ like $[Cu(bpy)]^+$, and rate constant is 0.0269 ms^{-1}.

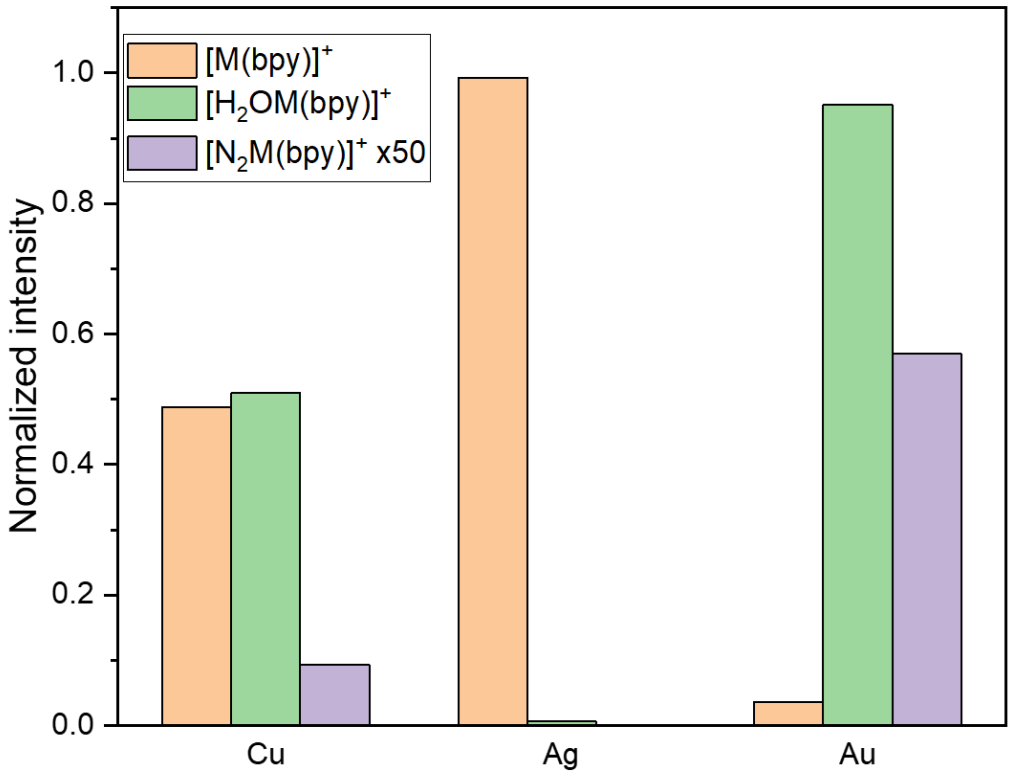

Figure 3.10 Comparison of the normalized intensity of reactants and products for different metal complexes after reaction goes for 100 ms. The intensity of nitrogen adducts is magnified with 50 times for clarity.

Figure 3.10 summarized the reactivity of different metal complexes under 100 ms reaction time. As shown on this graph, after reaction happens the same time, 50% of $[Cu(bpy)]^+$ gets reacted, but less than 10% of $[Au(bpy)]^+$ gets reacted, $[Au(bpy)]^+$ gets more than 90% reacted. Compare the intensity of water adducts, gold complex forms most of water adduct and silver complex forms the least water adduct (less than 1%). For nitrogen adduct, gold complex produces the most and then the copper complex. No nitrogen adduct is observed in the reaction of silver complex, which may either because the silver complex has a poor interaction with nitrogen gas, or because the $[N_2Ag(bpy)]^+$ is unstable that the product quickly break up after formation. In summary, $[Au(bpy)]^+$ is the most reactive reagent followed by $[Cu(bpy)]^+$ and $[Ag(bpy)]^+$, and $[Au(bpy)]^+$ has the highest binding ability with water and nitrogen gas. For all the metals, they show higher binding activity towards water gas than nitrogen gas.

3.3 Theory calculations

3.3.1 Structure optimization

Geometry for the reactants and products are optimized with DFT calculations. Optimized structures for both reactants and products are showed in Figure 3.11 and representative bond lengths are summarized in Table 3.1. Figure 3.11 shows that all bindings with gas molecules are through single dentate interaction. Length between metal to new attached gas molecules which can be seen as a new ligand to the metal-bipyridyl complex are calculated and presented by P. K. Chattaraj group[44] (numbers showed in parentheses). Compared with reported numbers, the results in this work are pretty similar to the numbers showed in paper, with a maximum difference of 0.003 Å, which means the methods used in this research works well. In terms of the orientation of the structures, the bare copper complex shows a nearly symmetrical structure with a dihedral angle of N_1-C-C-N_2 0.82 degrees. After binding with a water, the bond difference increases to 0.007 Å,

but the dihedral angle decreases to0.43 degrees. When nitrogen addicted to copper complex, it changes the length of the two Cu-N bonds simultaneously, so it keeps an overall symmetrical structure for the product, and the nitrogen adduct complex gets a more planar structure with the

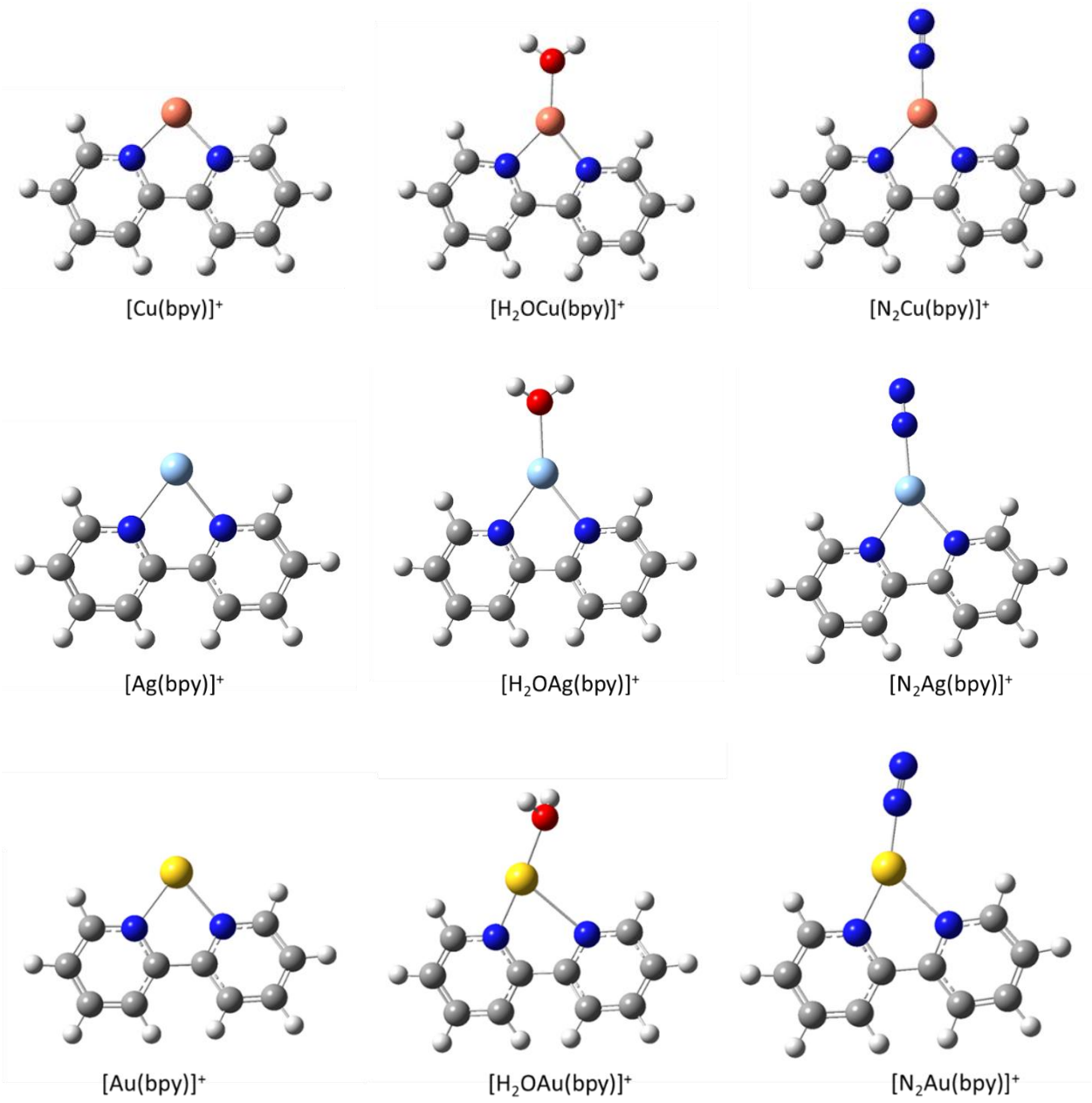

Figure 3.11 Geometry prediction for both bare metal complexes and gas attached metal complexes. Color codes for structures are Grey = C, White = H, Dark Blue = N, Red = O, Pink = Cu, Light Blue = Ag, Yellow = Au.

Table 3.1 Representative bond lengths (in Å) and angles (in degrees) for optimized structures. Length for metal to one nitrogen of bipyridine (M-N_1), length for metal to the other nitrogen of bipyridine (M-N_2), distance difference (Δd) between length for M-N_1 and M-N_2, length for metal to new attached molecules (M-L), the dihedral angle created by N_1-C-C-N_2 (in degrees) are calculated at PBE0/cc-pVTZ/cc-pVTZ-PP level. Numbers in parentheses are results reported by literature. (ref 44)

Complexes	M-N_1	M-N_2	Δd	M-L	Dihedral angle
$[Cu(bpy)]^+$	1.967	1.967	0.000		0.82
$[H_2OCu(bpy)]^+$	2.015	2.008	0.007	1.954 (1.954)	0.43
$[N_2Cu(bpy)]^+$	1.998	1.998	0.000	1.831 (1.830)	0.25
$[Ag(bpy)]^+$	2.254	2.255	0.001		14.33
$[H_2OAg(bpy)]^+$	2.275	2.279	0.004	2.227 (2.225)	12.96
$[N_2Ag(bpy)]^+$	2.251	2.250	0.001	2.122 (2.119)	2.43
$[Au(bpy)]^+$	2.221	2.223	0.002		13.94
$[H_2OAu(bpy)]^+$	2.029	2.675	0.646	2.097 (2.095)	27.56
$[N_2Au(bpy)]^+$	2.104	2.418	0.314	1.961 (1.962)	2.64

dihedral angle near 0. All silver complexes get similar shapes with copper complexes. $[Ag(bpy)]^+$ is a rather symmetrical shape, and water makes the structure a little unsymmetrical while nitrogen does not change the symmetry of structure. Besides, the adduct makes the structure access to a planar shape, and nitrogen addicted structure gets more planar than water addicted structure. For gold complexes, the structures show much different properties. The bare gold complex $[Au(bpy)]^+$ shows a nearly symmetrical structure with a length difference of 0.002 Å of two Au-N bonds. When binding with water, the structure of the adduct becomes more unsymmetrical and distorted compared to the bare gold complex, as the bond difference is up to 0.646 Å and dihedral angle is 27.56 degrees. When binding with nitrogen, nitrogen makes the bipyridine ligand less distorted with the dihedral angle of N_1-C-C-N_2 ranging from 13.94 degrees to 2.64 degrees, but still makes the whole structure less asymmetrical than water adduct.

The asymmetrical structure of tridentate gold(I)-bipyridine complex has also been observed by other groups[47-49]. Landis and Weinhold[50-51] believe the asymmetrical binding of bipyridine ligand is a manifestation of the anti-chelate effect, which occurs between the Au^+ center and the ligands. When a new ligand approaches the $[Au(bpy)]^+$, the anti-chelate effect arises from the fixed angle of the bipyridine ligand and the Au center prefers a linear geometry to satisfy the three-center four-electron (3c/4e) N-Au-L bond (where L represents the new attached ligand). Lucy M. C. Luong et al.[48] describe the symmetrical three dentate gold complexes as a transition state between the two limiting unsymmetrical structures. They interpret the 3c/4e bond with natural resonance theory (NRT) and "12 electron rule" formalism where only the 5d and 6s valance orbitals taking into consideration. Either nitrogen in the bipyridine ligand will donate the lone electron pair to an empty Au-L antibonding orbital, producing a 3c/4e N-Au-L bond. The 3c/4e bonding interaction maximizes when three atoms reach a linear geometry.

Plot showing the electron density helps better explain the symmetry of the structure. For $[N_2Cu(bpy)]^+$, p-orbital of both nitrogen in bipyridine overlap well with the d-orbital of copper as well as the p-orbital in nitrogen gas, the lone pair on nitrogen in bipyridine can easily delocalize along N-Cu-N bond, the symmetrical properties make the overall structure of copper complex symmetrical. $[N_2Ag(bpy)]^+$ has similar orbital formation as $[N_2Cu(bpy)]^+$ but the energy of orbital is overall lower than $[N_2Cu(bpy)]^+$. The orbitals showed here are all HOMO orbitals, except for $[N_2Ag(bpy)]^+$, which is HOMO-1 orbital. However, for $[N_2Au(bpy)]^+$, only one side of the p-orbital of nitrogen in bipyridine overlaps well with d orbital of Au and p-orbital of addicted nitrogen, making one nitrogen in bipyridine easy to donate the lone pair to the empty anti-binding orbital of nitrogen gas, forming a 3c/4e therefore. The difference between gold complex and copper complex may result from the bigger size of gold atom, with the fixed angle of bipyridine, the

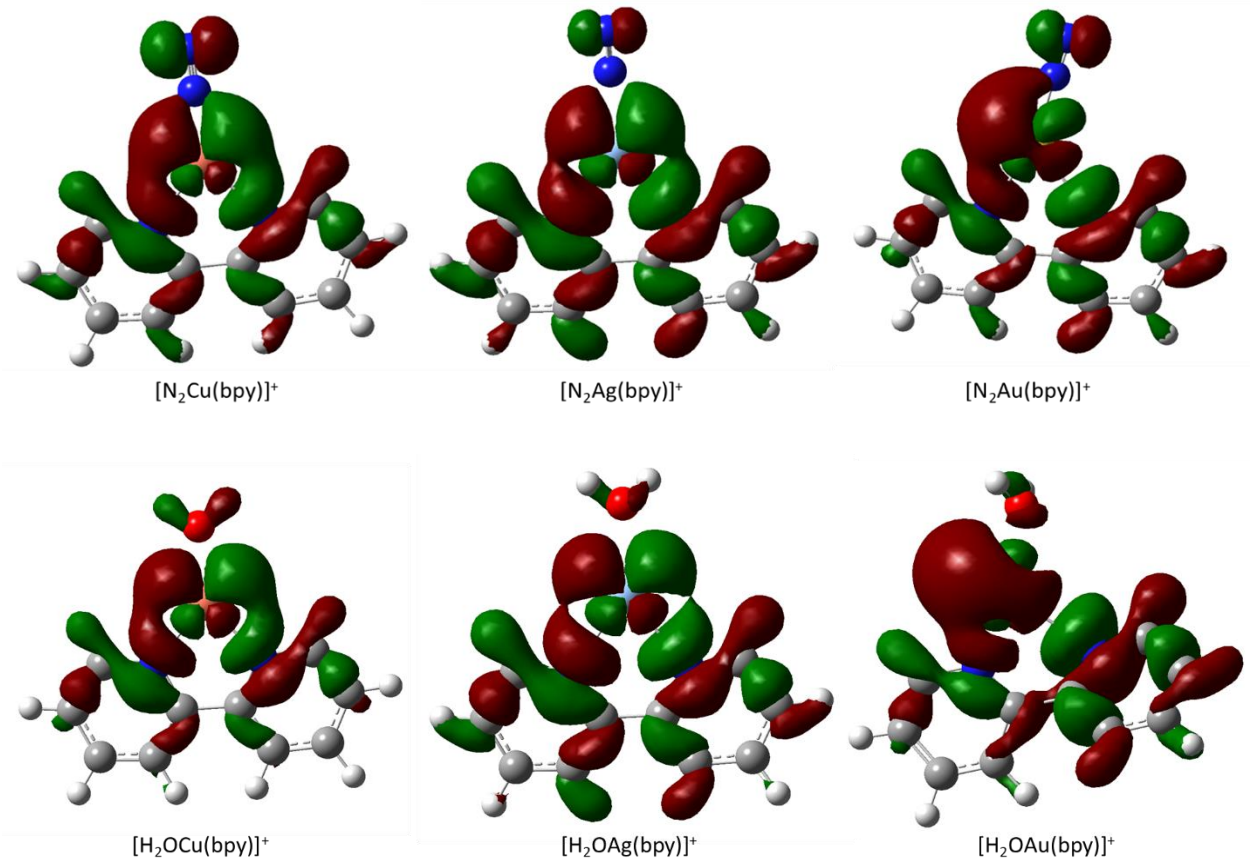

Figure 3.12 Molecular orbital for nitrogen adducts (top row) and water adducts (bottom row). HOMO are showed here except for $[N_2Ag(bpy)]^+$, where the HOMO-1 is showed here. Isovalue is 0.2 for all orbitals presented.

orbitals of both nitrogens cannot fully overlap with the orbitals of gold, instead, with some distortion of bipyridine, one nitrogen can form bond with gold, the other nitrogen prefers an anti-binding with gold orbital, therefore, the gold complex presents an asymmetrical shape. Explanation about the symmetrical $[H_2OCu(bpy)]^+$, $[H_2OCu(bpy)]^+$ and unsymmetrical $[H_2OAu(bpy)]^+$ are pretty similar to the nitrogen adducts, which depends on either one or two nitrogen orbitals in bipyridine overlap with the orbital of metals. For each metal, the lone pair on nitrogen can flow to the empty anti-bonding orbital of water.

3.3.2 Bond energies and thermo stability

The stability of adduct complexes is examined with different aspects. Table 3.2 shows the bond dissociation energy (BDE) of the M-L bond, the enthalpy change and energy change for the dissociation process of bound complexes. Numbers showed in parentheses are reported results.

Table 3.2. Bond Dissociation Energy (BDE, kcal/mol) for M-L bond, enthalpy change (ΔH, kcal/mol) at 298 K and Gibs Free Energy change (ΔG, kcal/mol) at 298 K for the Dissociation Reaction $[LM(bpy)]^+ \rightarrow [M(bpy)]^+ + L$ at PBE0/cc-pVTZ/cc-pVTZ-PP level, numbers in parentheses are results reported by Chattaraj, P. K. Group. (ref 44)

Complexes	BDE	ΔH	ΔG
$[Cu(bpy)]^+$			
$[H_2OCu(bpy)]^+$	26.5 (18.9)	27.1 (21.0)	18.5 (13.3)
$[N_2Cu(bpy)]^+$	21.6 (21.9)	22.2 (23.3)	12.7 (13.8)
$[Ag(bpy)]^+$			
$[H_2OAg(bpy)]^+$	20.4 (12.7)	21.0 (14.8)	12.9 (7.3)
$[N_2Ag(bpy)]^+$	11.5 (12.1)	12.1 (13.0)	4.7 (5.3)
$[Au(bpy)]^+$			
$[H_2OAu(bpy)]^+$	30.1 (20.9)	30.7 (24.2)	20.5 (15.4)
$[N_2Au(bpy)]^+$	24.2 (24.6)	24.8 (25.9)	15.8 (17.7)

Compared to the reported energies, the nitrogen addicted complexes get similar energies with literature, and the differences are among 0.1 to 0.9 kcal/mol lower than reported. However, the water addicted complexes calculated in this research usually have a 5-6 kcal/mol energy higher than the reported energies. For comparison, typical hydrogen bonds have energies of 1-20 kcal/mol in different environmental conditions.[52] One possible reason that cause this difference may be the energy correction for the calculations, the literature did both Zero Point Energy (ZPE) correction and Basis Set Superposition Error (BSSE) correction to the energy calculations, but only ZPE correction applied to the energies in this work. ZPE[53] is the lowest possible energy that a quantum system may have, because of the truth that all quantum system undergoes fluctuation at each

energy level, zero-point energy must be included when calculating the ground state energy, which is a consequence of wave-like nature.

BSSE[54] is an error that often exists in calculation of intermolecular energies. For the reaction A + B → AB, the interaction cannot be simply calculated by E(AB)-E(A)-E(B). Because the decrease of energy of AB will not only result from the interaction between A and B which is really needed, but also the overlap functions from A and B, which increases the basis set used to calculate the energy of AB. Therefore, a BSSE correction should be included, and the energy should be calculated as E(AB)-E(A)-E(B)+E(BSSE). However, whether to do correction to BSSE is a controversial problem, some researchers[55] prefer applying correction to BSSE especially when the interactions are weak, while some[56] argue that the error can be neglected if the right basis sets are selected. In this research, calculation without BSSE correction can better support the experimental observation. For the given metal, M-O bonds in water adducts have higher bond dissociation energy than the M-N bonds in nitrogen adducts. Besides, the enthalpy change of the dissociation process are all positive, which means dissociation is an endothermic process for all bound complexes. Enthalpy change of dissociation for water adducts are also higher than nitrogen adducts, indicating the water adducts needs higher energy to dissociate. The dissociation processes of bound complexes are nonspontaneous because ΔG are greater than 0. In summary, the water adducts are more stable than nitrogen adducts. Compare the stability between different metal complexes, the gold complexes have a higher bond dissociation energy and higher enthalpy, followed by copper and silver, for both the two gases. which means $[Au(bpy)]^+$ has higher binding ability with gas molecules, which is consistent with the experimental results.

3.3.3 Activation of bonds

During the process $[M(bpy)]^+$ binding with nitrogen or water, the metal complexes also work like a bond activation reagent to the bonds of the small gas molecules. The length of N≡N and H-O bonds get elongated with different degrees (ranges from 0.001 Å to 0.004 Å) in the complexes compared with the length in free gas molecules (Table 3.3 and Table 3.4). The shape of water keeps symmetrical all the way during the whole process, so one bond length showed in table. $[Au(bpy)]^+$ makes the O-H bond prolong the most with 0.005 Å, and $[Au(bpy)]^+$ and $[Cu(bpy)]^+$ both make N≡N prolong about 0.004 Å.

Table 3.3 The bond length of O-H (Å) in free H_2O and in different water adducts, the length elongated (Å) of O-H bond in adducts compared with free water.

Name	Length of O-H	Length elongated
H_2O	0.958	
$[H_2OCu(bpy)]^+$	0.960	0.002
$[H_2OAg(bpy)]^+$	0.960	0.002
$[H_2OAu(bpy)]^+$	0.963	0.005

Table 3.4 The bond length of N≡N (Å) in free N_2 and in different adducts, the length elongated (Å) of N≡N bond in adducts compared with free N_2.

Name	Length of N≡N	Length elongated
N_2	1.090	
$[N_2Cu(bpy)]^+$	1.094	0.004
$[N_2Ag(bpy)]^+$	1.091	0.001
$[N_2Au(bpy)]^+$	1.094	0.004

Table 3.5 Prediction of IR frequency (cm^{-1}) of O-H bond for water symmetrical stretch and the decreased frequency (cm^{-1}) of O-H stretch in complexes compared with free water.

Name	Frequency/cm^{-1}	Decreased frequency/cm^{-1}
H_2O	3865.60	
$[H_2OCu(bpy)]^+$	3851.58	14.02
$[H_2OAg(bpy)]^+$	3849.46	7.14
$[H_2OAu(bpy)]^+$	3809.84	55.76

Table 3.6 Prediction of IR frequency (cm^{-1}) of N≡N bond for symmetrical stretch and the decreased frequency (cm^{-1}) of N≡N stretch in complexes compared with free N_2.

Name	Frequency/cm^{-1}	Decreased frequency/cm^{-1}
N_2	2482.56	
$[N_2Cu(bpy)]^+$	2423.10	59.46
$[N_2Ag(bpy)]^+$	2464.91	17.65
$[N_2Au(bpy)]^+$	2427.64	54.92

IR calculates the frequency of each movement. For O-H bond of water, the symmetrical stretch frequency is discussed here. All metal complexes make a significant shift to a lower frequency, and gold complex makes frequency shift the most. Along with the result of bond elongation, $[Au(bpy)]^+$ is the best candidate for O-H activation. For N≡N bond of nitrogen, compared with the symmetrical stretch frequency in the free nitrogen gas molecule, there is also a red-shift of the frequency for N≡N stretch, and in the copper complexes, the frequency shifts the most. Therefore, $[Cu(bpy)]^+$ performs the best on nitrogen bond activation. Silver complexes is the least active reagent for either O-H or N≡N activation.

3.4 Prediction effect of ligands

Phenanthroline (in short of phen) is also a common ligand used in coordination chemistry. It is used in this research as a substitution of bipyridine to study how the ligand will affect interaction between metal complex and gas molecules.

The geometries after optimization are showed in Figure 3.13. The orientation of the structures follows similar tendency as bipyridine coupled complexes. All complexes have a single dentate binding with gas molecules. For copper and silver complexes, they have relative symmetrical structures, but for gold complexes, their structures are unsymmetrical. The difference between these structures with bipyridine structures are that these structures are not distorted, which is mainly due of the rigidity of Phenanthroline.

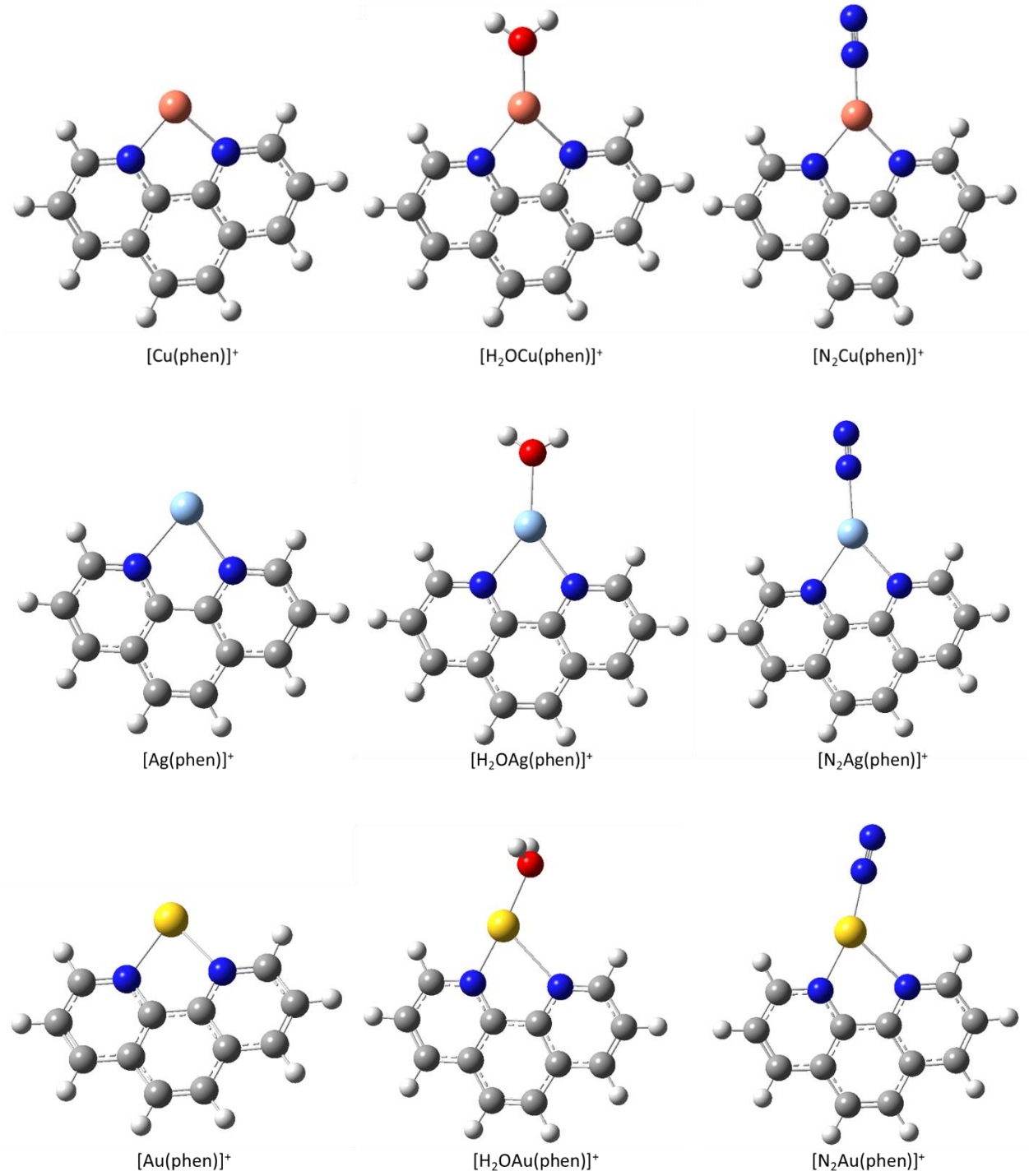

Figure 3.13 Optimized geometry for the bare $[M(phen)]^+$ and gas attached complexes. Color codes for structures are Grey = C, White = H, Dark Blue = N, Red = O, Pink = Cu, Light Blue = Ag, Yellow = Au.

Table 3.7 Bond Dissociation Energy (BDE, kcal/mol) for M-L bond, enthalpy change (ΔH, kcal/mol) at 298 K and Gibs Free Energy change (ΔG, kcal/mol) at 298 K for the Dissociation Reaction $[LM(phen)]^+ \rightarrow [M(phen)]^+ + L$ at PBE0/cc-pVTZ/cc-pVTZ-PP level.

Complexes	BDE	ΔH	ΔG
$[Cu(phen)]^+$			
$[H_2OCu(phen)]^+$	25.9	26.5	18.1
$[N_2Cu(phen)]^+$	20.9	21.5	12.4
$[Ag(phen)]^+$			
$[H_2OAg(phen)]^+$	20.1	20.7	12.3
$[N_2Ag(phen)]^+$	11.3	11.9	3.6
$[Au(phen)]^+$			
$[H_2OAu(phen)]^+$	29.6	30.2	20.7
$[N_2Au(phen)]^+$	23.9	24.5	14.8

Thermostability is also calculated using the same method as bipyridine. The results are unbelievably similar to the results of bipyridine, with energies for all complexes are less than 1 kcal/mol lower than bipyridine complexes. Which indicates $[M(phen)]^+$ complexes may have similar interactions with the gas molecules like $[M(bpy)]^+$.

The molecular orbitals of $[M(phen)]^+$ help rationale why $[M(phen)]^+$ performs so close to $[M(bpy)]^+$. As hypothesized, the orbital overlap of p orbital of nitrogen in the ligand, the d orbital of metal and the anti-bonding orbital allows nitrogen to donate lone pair to the empty orbital of gas molecules, so that create the interaction with the gas molecules. And from the graph, it is clear to see that phen creates similar orbital overlap as bipy, so that establish similar interactions with gas molecules. Because middle benzene ring is an electron-withdrawing group, which makes the electron density on nitrogen slightly goes down, therefore, the interaction between $[M(phen)]^+$ with gas molecule is slightly weaker than $[M(bpy)]^+$. And due to the big size of Au orbital, it cannot overlap well with both p orbitals of nitrogen in phen, thus getting an unsymmetrical geometry.

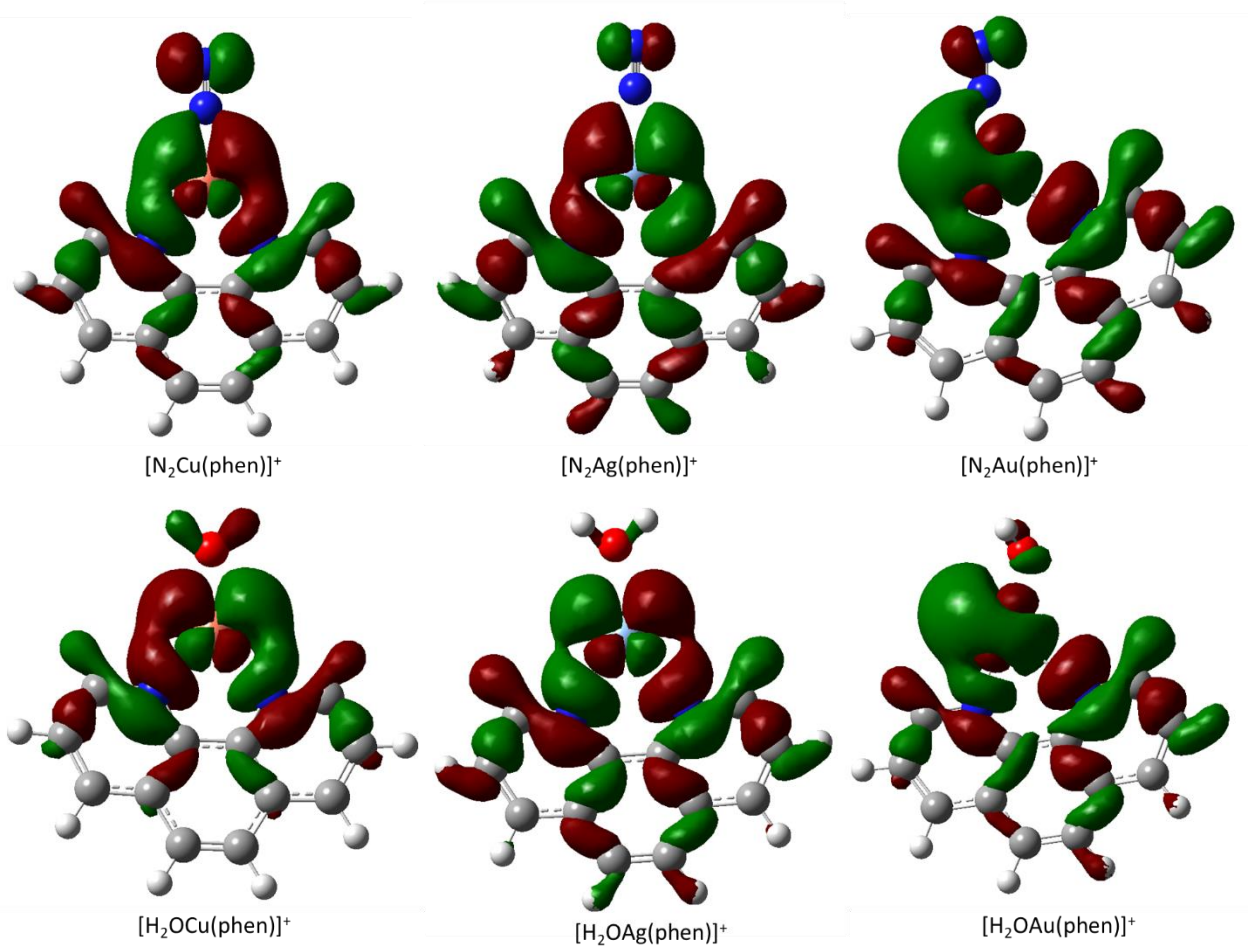

Figure 3.14 Molecular orbitals for $[M(phen)]^+$ complexes. HOMOs are showed for copper and gold complexes, HOMO-1 are showed for silver complexes. Isovalue is 0.2 for all orbitals presented.

CHAPTER IV: CONCLUSIONS AND FUTURE WORK

4.1 Conclusions

This research extended the study of metal-bipyridine (metal = Cu, Ag, Au) system to the gas phase, synthesized the single charged metal-bipyridine ion $[M(bpy)]^+$ and compared the reactivity of different metal complexes for the reaction with small gas molecules, N_2 and H_2O. The experimental results show that $[Au(bpy)]^+$ has the highest binding ability with both the N_2 and H_2O, followed by is $[Cu(bpy)]^+$, and $[Ag(bpy)]^+$ has the weakest interaction with H_2O and no interaction with N_2 is observed, which may because the indeed weak interaction with N_2, or the nitrogen adduct is not stable.

Kinetic study shows that the reactions follow pseudo-first order with respect to the metal complex $[M(bpy)]^+$ for Cu and Au, Ag does not show a good reaction order regression, which may because of the signal fluctuation due to the low reactivity of $[Ag(bpy)]^+$, but there is high probability that the reaction between $[Ag(bpy)]^+$ and gas molecules also follows the pseudo-first order, based on the properties of $[Ag(bpy)]^+$.

DFT calculations are applied to find more properties. Geometry optimization finds that for all complexes, they form a single dentate with gas molecules. Optimized structures for copper complexes and silver complexes show a relative symmetrical shape, the gold complexes show obvious unsymmetrical structures after binding with a gas molecule. Molecular orbital plots help explain the phenomenon and give a deeper insight to the interaction between metal complexes and gas molecules. The overlap of orbital allow nitrogen in bipyridine donating the electrons to the anti-bonding of gas molecule, creating an interaction between them. And the degree of orbital overlap determines the interaction.

Calculated thermo parameters show that the products of the reaction are rather stable. Dissociation of products is endothermic and nonspontaneous. Bond dissociation energy shows that $[Au(bpy)]^+$ has the highest binding ability with gas molecules, followed by $[Cu(bpy)]^+$ and $[Ag(bpy)]^+$. For all of the metal complexes, they have higher binding ability towards H_2O than N_2, which agrees with the experiment results.

IR spectrum of products are also predicted. IR shows that all metal complexes have some ability to active the N≡N bond and O-H bond. Compared of the frequency, there is significant red-shift for the symmetrical stretching of bonds. Besides, the bond lengths also get elongated compared with the length in free gas. $[Au(bpy)]^+$ works the best on O-H activation, and $[Cu(bpy)]^+$ works the best on N≡N activation.

In the end, phenanthroline is used to study how ligand will affect the interaction between complex and gases with calculations. It is predicted that M-phen complexes have similar geometry as M-bpy. The interactions between $[M(phen)]^+$ with gas molecules are much similar to $[M(bpy)]^+$ but they are slightly lower than $[M(bpy)]^+$. Molecular orbitals showed to provide interpretations. The similar orbital overlap explains the similarity between two series of complexes. And the lower electron density on nitrogen of phenanthroline may contribute to the slightly weaker interactions for $[M(phen)]^+$.

4.2 Future work

Future work can be divided to two branches, the theoretic study and applications.

For the theoretic study, further study may focus on the study of effect of other metals or ligands. Platinum is the metal with the highest oxidation potential, so the Platinum complexes may have higher reactivity than coinage metal in the gas phase. There is already literature[57] reported that

Platinum can also be oxidized during electrospray ionization, so the platinum complexes could be synthesized with electrospray.

For the ligand effect, part of the ligand effect has been predicted in this thesis. Experimental data can be acquired to check if this prediction works. Other ligands either with electron-withdrawing group or electron-donating group can also been studied to see how it will affect the interaction between complexes and gas molecules.

For the application, the metal complexes in this research are promising to be the key ingredient of a gas sensor. The metal complexes in this research are pretty sensitive to the gases. As is shown at the beginning, the pressure inside Ion Trap is only $1 * 10^{-5}$ Torr, with 99% of it are He gas, so there is extremely low concentration of nitrogen gas and water gas. However, the metal complexes can still bind with gas molecules and get detected. The metal complexes also have the potential to detect other gases. Moreover, many metal complexes in the solution phase works as a catalyst[34,58], the metal complexes in the gas phase may also work to catalyze the reactions in the gas phase. Other studies in solution phase like the photochemistry[59] can also be studied in gas phase.

LIST OF REFERENCES

1. Brodbelt, J. S., Analytical Applications of Ion-molecule Reactions. *Mass Spectrom. Rev.* **1997,** 16, 91-110.

2. Munson, M. S. B. F., F. H., Chemical Ionization Mass Spectrometry. I. General Introduction. *J. Am. Chem. Soc.* **1966,** 88 (12), 2621-2630.

3. Baratta, W.; Da Ros, P.; Del Zotto, A.; Sechi, A.; Zangrando, E.; Rigo, P., Cyclometalated Ruthenium(II) complexes as highly active transfer hydrogenation catalysts. *Angew. Chem. Int. Ed. Engl.* **2004,** 43 (27), 3584-8.

4. Gronert, S., Gas Phase Studies of the Competition between Substitution and Elimination Reactions. *Acc. Chem. Res.* **2003,** 36, 848-857.

5. Manikandan, P.; Zhang, J.; Hase, W. L., Chemical dynamics simulations of X^- + CH_3Y --> XCH_3 + Y^- gas-phase S(N)2 nucleophilic substitution reactions. Nonstatistical dynamics and nontraditional reaction mechanisms. *J. Phys. Chem. A* **2012,** 116 (12), 3061-80.

6. Fiebig, L.; Kuttner, J.; Hilt, G.; Schwarzer, M. C.; Frenking, G.; Schmalz, H. G.; Schafer, M., Cobalt catalysis in the gas phase: experimental characterization of cobalt(I) complexes as intermediates in regioselective Diels-Alder reactions. *J. Org. Chem.* **2013,** 78 (20), 10485-93.

7. Eberlin, M. N. C., R. Graham, Polar [4+2] Diels-Alder Cycloadditions of Acylium Ions in the Gas Phase. *J. Am. Chem. Soc.* **1993,** 115, 9226-9233.

8. McDonald, R. N. C., Kasem; Setter, D. W., Hypovalent Radicals. 4. Gas-Phase Studies of the Ion-Molecule Reactions of Cyclopentadienylidene Anion Radical in a Flowing Afterglow. *J. Am. Chem. Soc.* **1980,** 102, 6491-6498.

9. Iino, T.; Ohashi, K.; Inoue, K.; Judai, K.; Nishi, N.; Sekiya, H., Infrared spectroscopy of $Cu^+(H2O)_{(n)}$ and $Ag^+(H2O)_{(n)}$: coordination and solvation of noble-metal ions. *J. Chem. Phys.* **2007,** 126 (19), 194302.

10. Feyel, S.; Dobler, J.; Schroder, D.; Sauer, J.; Schwarz, H., Thermal activation of methane by tetranuclear $[V_4O_{10}]^+$. *Angew. Chem. Int. Ed. Engl.* **2006,** 45 (28), 4681-5.

11. Bernhardt, T. M., Gas-phase kinetics and catalytic reactions of small silver and gold clusters. *Int. J. Mass Spectrom.* **2005,** 243 (1), 1-29.

12. Beyer MK. Hydrated metal ions in the gas phase. *Mass Spectrom. Rev.* **2007,** 26 (4), 517-541.

13. Assis AC, Couto N, Duarte MF, et al. Azidoacetone as a complexing agent of transition metals Ni_2^+/Co_2^+ promoted dissociation of the C-C bond in azidoacetone. *J. Mass Spectrom.* **2011,** 46 (7), 696-704.

14. R. G. Cooks, H. C., Marcos N. Eberlin, Xubin Zheng, W. Andy Tao, Polar Acetailization and Transacetalization in the Gas Phase: The Eberlin Reaction. *Chem. Rev.* **2006,** 106, 188-211.

15. Li, H.; Li, F.; Han, C.; Cui, Z.; Xie, G.; Zhang, A., Highly efficient gas-phase reactivity of protonated pyridine radicals with propene *Phys. Chem. Chem. Phys.* **2017,** 19, 31072.

16. Eberlin MN. Electrospray Ionization Mass Spectrometry: A Major Tool to Investigate Reaction Mechanisms in Both Solution and the Gas Phase. *Eur. J. Mass Spectrom.* **2007,** 13(1),19-28.

17. Santos, L. S.; Pavam, C. H.; Almeida, W. P.; Coelho, F.; Eberlin, M. N., Probing the mechanism of the Baylis-Hillman reaction by electrospray ionization mass and tandem mass spectrometry. *Angew. Chem. Int. Ed. Engl.* **2004,** 43 (33), 4330-4333.

18. Gustavsson, S. A. Samskog, J.; Markides, K. E.; Langstrom B., Studies of signal suppression in liquid chromatography-electrospray ionizataion mass spectrometry using volatile ion-pairing reagents. *J. Chromatogr. A* **2001,** 937, 41-47.

19. Vachet, R. W., Callahan, J. H., Quadrupole ion trap studies of the structure and reactivity of transition metal ion pair complexes. *J. Mass Spectrom.* **2000,** 35, 311-320.

20. Meyer, J.; Wester, R., Ion-Molecule Reaction Dynamics. *Annu. Rev. Phys. Chem.* **2017,** 68, 333-353.

21. Bohme, D. K.; Mackay, G. I., Bridging the gap between the gap-phase and solution-transition in the kinetics of nucleophilic displacement-reactions. *J. Am. Chem. Soc,* **1981,** 103, 978-979.

22. Viggiano, A. A.; Arnold, S. T.; Morris, R. A.; Ahrens, A. F.; Hierl P. M., Temperature dependences of the rate constants and branching ratios for the reactions of $OH^-(H_2O)_{0-4} + CH_3Br$. *J. Phys. Chem.* **1996,** 100, 14397-14402.

23. Raugei, S., Cardini, G.; Schettino, V., Microsolvation effect on chemical reactivity: The case of $Cl^- + CH_3Br$ S_N2 reaction. *J. Chem. Phys.* **2001,** 114 (9), 4089-4098.

24. Yu, F., Dynamic exit-channel pathways of the microsolvated $HO^-(H_2O) + CH_3Cl$ S_N2 reaction: Reaction mechanisms at the atomic level from direct chemical dynamics simulations. *J. Chem. Phys.* **2018,** 148 (1), 014302.

25. Paul, W.; Steinwedel, H., A New Mass Spectrometer without a Magnetic Field. *Z. Naturforsch* **1953,** 8a, 4480-450

26. Stafford, G. C.; Kelley, P. E.; Syka, J. E. P.; Reynolds, W. E.; Todd, J. F. Recent Improvements In and Analytical Applications of Advanced Ion Trap Technology. *Int. J. Mass Spectrom. Ion Proc.* **1984,** 60, 85-98.

27. Stafford, G., Ion Trap Mass Spectrometry: A Personal Perspective. *Am. Soc. Mass Spectrom.* **2002,** 13, 589-596.

28. Jae C. Schwartz, M. W. S., A Two-Dimensional Quadrupole Ion Trap Mass Spectrometer. *Am. Soc. Mass Spectrom.* **2002,** 13, 659-669.

29. Scott T. Quarmby, R. A. Y., Fundamental studies of ion injection and trapping of electrosprayed ions on a quadrupole ion trap. *Int. J. Mass Spectrom.* **1999,** 81, 190-191.

30. Yoshinari, K., Theoretical and numerical analysis of the behavior of ions injected into a quadrupole ion trap mass spectrometer. *Rapid commun. mass spectrom.* **2000,** 14, 215-223.

31. Koo, B. K. Synthesis, Crystal structure, and Characterization of Copper (II) Acetate Complex. *Bull. Kor. Chem. Soc.* **2001,** 22, 113-117

32. Das, A. P. S. C. P. M. C., A Phosphate‐Based Silver–Bipyridine 1D Coordination Polymer with Crystallized Phosphoric Acid as Superprotonic Conductor. *Chem. Eur. J.* **2020,** 26 (20), 4607-4612.

33. Kandaian, S.; Huebner, R.; Jansen, M. Electrocrystallisation and single crystal structure determination of Bis(2,2'-bipyridyl) silver(II) Perchlorate $[Ag(bipy)_2](ClO_4)_2$. *Polyhedron* **2012** 48, 68-71.

34. Barnett, S. M.; Goldberg, K. I.; Mayer, J. M., A soluble copper-bipyridine water-oxidation electrocatalyst. *Nat. Chem.* **2012,** 4 (6), 498-502.

35. Nikolaev, A.; Legault, C. Y.; Zhang, M.; Orellana, A., The Acid-Free Cyclopropanol-Minisci Reaction Reveals the Catalytic Role of Silver-Pyridine Complexes. *Org. Lett.* **2018,** 20 (3), 796-799.

36. Patel, R. N.; Singh, N.; Shukla, K. K.; Niclos-Gutierrez, J.; Castineiras, A.; Vaidyanathan, V. G.; Nair, B. U., Characterization and biological activities of two copper(II) complexes with diethylenetriamine and 2,2'-bipyridine or 1,10-phenanthroline as ligands. *Spectrochim. Acta. A* **2005,** 62, 261-268.

37. Corongiu, G.; Nava, P., Gas-phase geometries and energies of bis(2,2-bipyridine) interacting either with Cu(I) or Ag(I): Computational study. *Int. J. Quant. Chem.* **2003,** 93 (6), 395-404.

38. Xu, S.; Gozem, S.; Krylov, A. I.; Christopher, C. R.; Weber, J. M., Ligand influence on the electronic spectra of monocationic copper-bipyridine complexes. *Phys. Chem. Chem. Phys.* **2015,** 17 (47), 31938-31946.

39. Takano, S.; Tsukuda, T., Chemically Modified Gold/Silver Superatoms as Artificial Elements at Nanoscale: Design Principles and Synthesis Challenges. *J. Am. Chem. Soc.* **2021,** 143 (4), 1683-1698.

40. Solovyev, I. V.; Kondinski, A.; Monakhov, K. Y.; Koshevoy, I. O.; Grachova, E. V., Synthesis, photophysical properties and cation-binding studies of bipyridine-functionalized gold(I) complexes. *Inorg. Chem. Front.* **2018,** 5 (1), 160-171.

41. Li, A.; Luo, Q.; Park, S. J.; Cooks, R. G., Synthesis and catalytic reactions of nanoparticles formed by electrospray ionization of coinage metals. *Angew. Chem. Int. Ed. Engl.* **2014,** 53 (12), 3147-3150.

42. Torvinen, M.; Kalenius, E.; Sansone, F.; Casnati, A.; Janis, J. *J. Am. Soc. Mass Spectrom.* **2012,** 23, 359-365.

43. Wickens, J. R.; Sleeman, R.; Keely, B. J., Adduction of solvent molecules by ions isolated within an ion trap mass spectrometer under atmospheric pressure ionization conditions. *Rapid Commun. Mass Spectrom.* **2007,** 21 (15), 2491-2496.

44. Jana, G.; Pan, S.; Chattaraj, P. K., Binding of Small Gas Molecules by Metal-Bipyridyl Monocationic Complexes (Metal = Cu, Ag, Au) and Possible Bond Activations Therein. *J. Phys. Chem. A* **2017,** 121 (19), 3803-3817.

45. Adamo, C., Barone, V. Inexpensive and accurate predictions of optical excitations in transition-metal complexes: the TDDFT/PBE0 route. *Theor. Chem. Acc.* **2000,** 105, 169–172.

46. Shiels, O. J.; Kelly, P. D.; Bright, C. C.; Poad, B. L. J.; Blanksby, S. J.; da Silva, G.; Trevitt, A. J., Reactivity Trends in the Gas-Phase Addition of Acetylene to the N-Protonated Aryl Radical Cations of Pyridine, Aniline, and Benzonitrile. *J. Am. Soc. Mass Spectrom.* **2021,** 32 (2), 537-547.

47. Budzelaar, A. C. T. d. H. C. E. P. H. M., Between T and Y: Asymmetry in the Interaction of LAu(I) with Bipy and β-Diiminate-like Ligands. *Eur. J. Inorg. Chem.* **2021,** 4, 314-320.

48. Luong, L. M. C.; Aristov, M. M.; Adams, A. V.; Walters, D. T.; Berry, J. F.; Olmstead, M. M.; Balch, A. L., Unsymmetrical Coordination of Bipyridine in Three-Coordinate Gold(I) Complexes. *Inorg. Chem.* **2020,** 59 (6), 4109-4117.

49. Lopez-de-Luzuriaga, J. M.; Monge, M.; Olmos, M. E.; Rodriguez-Castillo, M.; Soldevilla, I.; Sundholm, D.; Valiev, R. R., Perhalophenyl Three-Coordinate Gold(I) Complexes as TADF Emitters: A Photophysical Study from Experimental and Computational Viewpoints. *Inorg. Chem.* **2020,** 59 (19), 14236-14244.

50. Landis, C. R.; Hughes, R. P. Weinhold, F. Bonding Analysis of $TM(cAAC)_2$ (TM = Cu, Ag and Au) and the Importance of Reference State. *Organometallics* **2015,** 34, 3442-3449.

51. Landis, C. R.; Weinhold, F. Valence and extra-valence orbitals in main group and transition metal bonding. *J. Comput. Chem.* **2007,** 28, 198-203.

52. Wendler, K.; Thar, J.; Zahn, S.; Kichner, B. Estimating the Hydrogen Bond Energy. *J. Phys. Chem. A* **2010,** 114, 35, 9529–9536.

53. Cosonka, B. R., Arienn; Perdew, J. P., Estimation, Computation, and Experimental Correction of Molecular Zero-Point Vibrational Energies. *J. Phys. Chem. A* **2005,** 109, 6779-6789.

54. Gutowski, M., The Basis Set Superposition Error in Correlated Electronic Structure Calculations. *Chem. Phys. Lett.* **1986,** 124 (4), 370-375.

55. Salvador, F. Paizs, B.; Duran, M.; Shuai, S., On the Effect of the BSSE on Intermolecular Potential Energy Surfaces. Comparison of a priori and a posteriori BSSE Correction Schemes. *J. Comput. Chem.* **2001,** 22 (7), 765-786.

56. Lin, Z.; Lu, T.; Ding, X. L., A theoretical investigation on doping superalkali for triggering considerable nonlinear optical properties of $Si_{12}C_{12}$ nanostructure. *J. Comput. Chem.* **2017,** 38 (18), 1574-1582.

57. Baksi, A.; Bag, S.; Kruk, R.; Nandam, S. H.; Hahn, H., Structural insights into metal-metalloid glasses from mass spectrometry. *Sci. Rep.* **2020,** 10 (1), 17467.

58. Henrion, G.; Chavas, T. E.; Le Goff, X.; Gagosz, F., Biarylphosphonite gold(I) complexes as superior catalysts for oxidative cyclization of propynyl arenes into indan-2-ones. *Angew. Chem. Int. Ed. Engl.* **2013,** 52 (24), 6277-82.

59. Marcinkowski, D.; Wałęsa-Chorab, M.; Patroniak, V.; Kubicki, M.; Kądziołka, G.; Michalkiewicz, B., A new polymeric complex of silver(I) with a hybrid pyrazine–bipyridine ligand – synthesis, crystal structure and its photocatalytic activity. *New J. Chem.* **2014,** 38 (2), 604-610.

Appendix

Appendix A: EIC curve of m/z 394

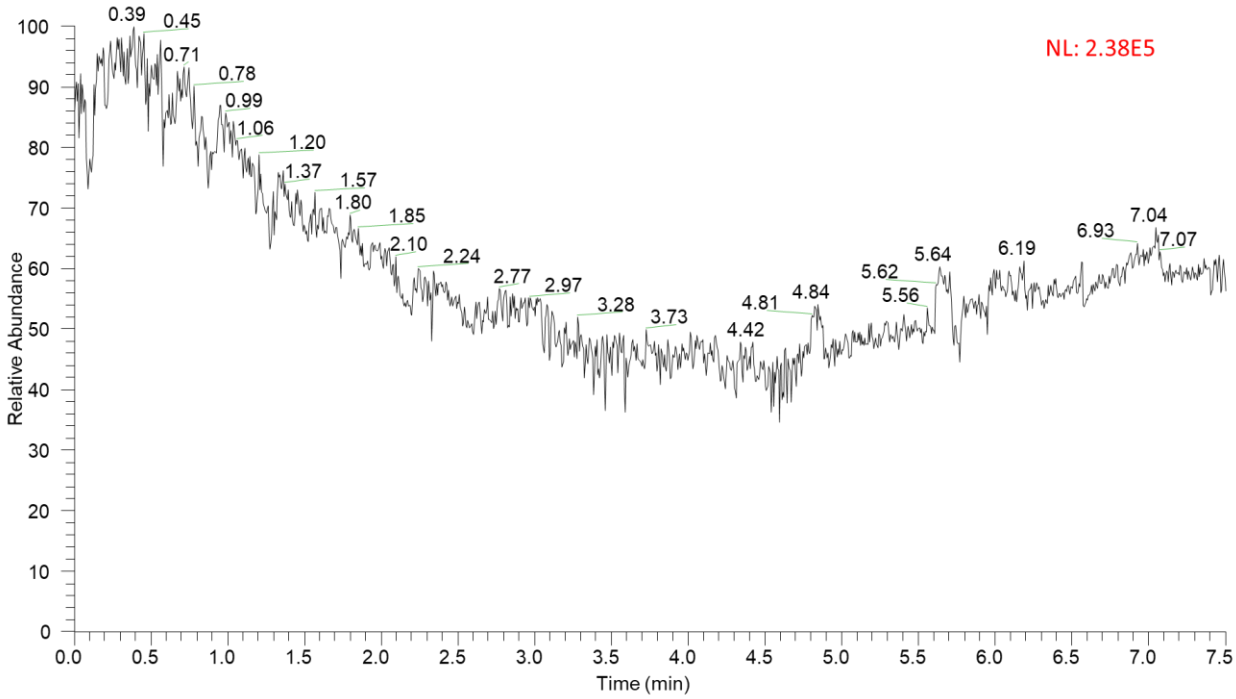

Appendix B: MS^2 of m/z 394 for the background peak and $[Au(bpy)]^+$

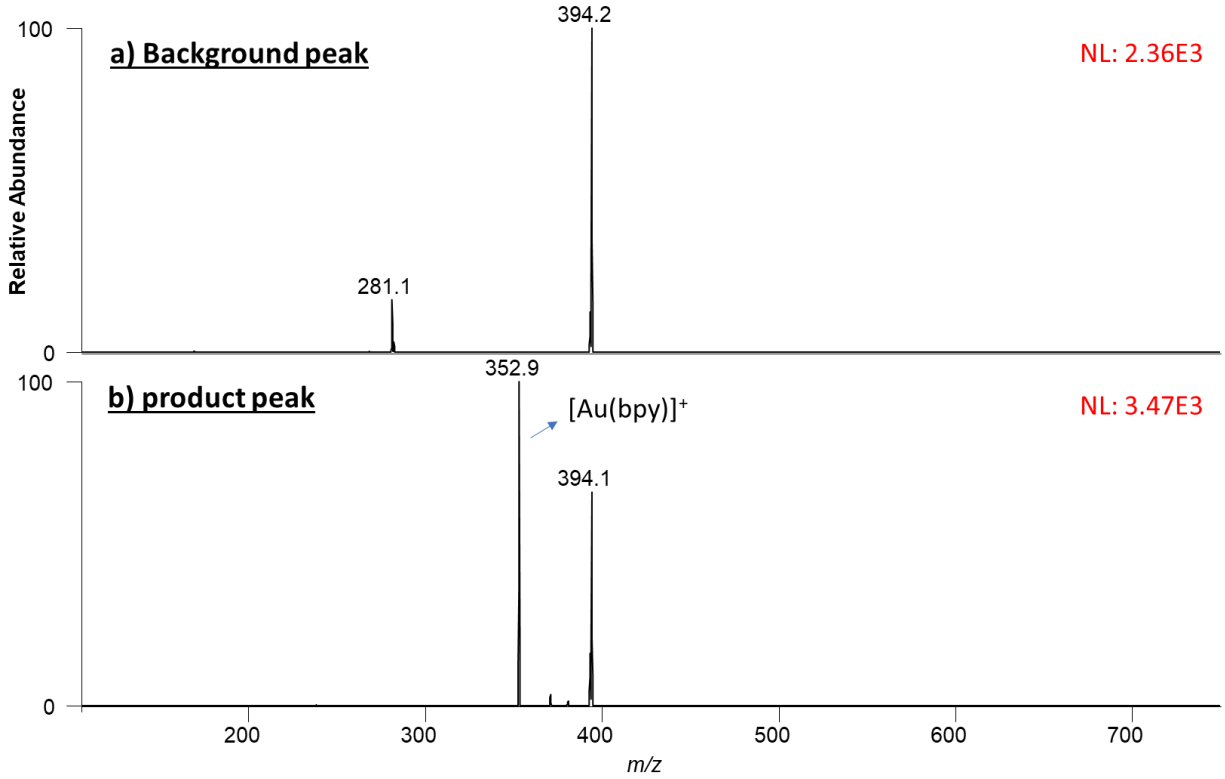

Appendix C: EIC curves that represents the time for signal appearance.

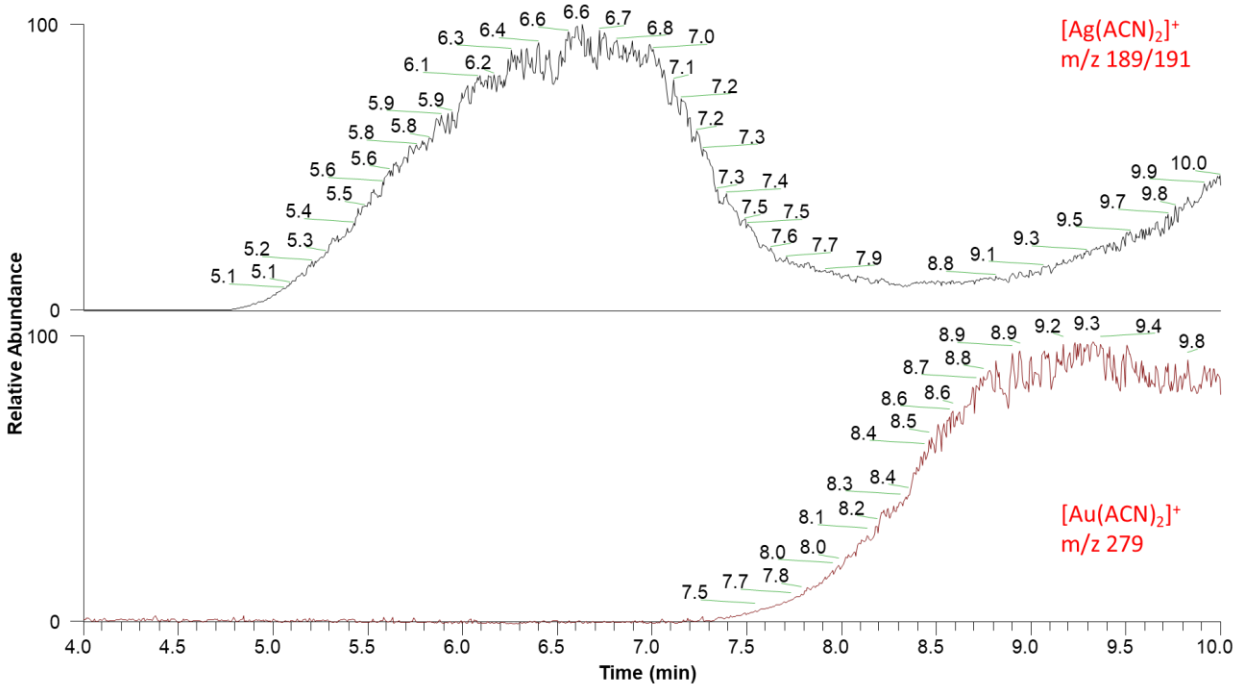

Appendix D: MS^2 spectrum of m/z 280

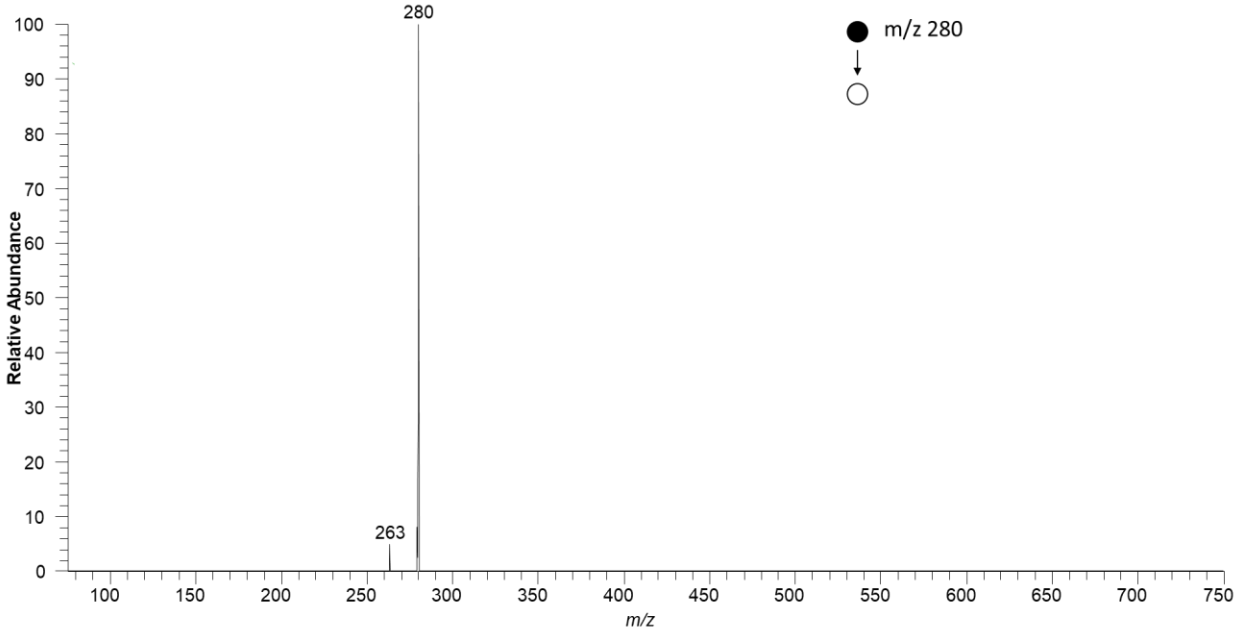

Appendix E: Geometry coordinate of the calculation output file

$[Cu(bpy)]^+$

	X	Y	Z
C	1.6664747829	1.4191628248	-0.8377667129
C	3.0134658022	1.4857633879	-1.1664131018
C	3.6694620088	2.7047554164	-1.1256870170
C	2.9688037421	3.8387100582	-0.7571694960
C	1.6296768063	3.7042955456	-0.4403644831
C	0.9046554435	0.1363538898	-0.8644178045
C	1.4923869879	-1.0646785951	-1.2372134386
C	0.7362284286	-2.2250310584	-1.2436673476
C	-0.5961099666	-2.1668130881	-0.8774961749
C	-1.1209649286	-0.9394058845	-0.5174409003
H	3.5590042220	0.5991268548	-1.4528885243
H	4.7200777933	2.7630371539	-1.3806875955
H	3.4411419134	4.8104845275	-0.7125998776
H	1.0390146803	4.5622518957	-0.1453456600
H	2.5323515260	-1.1075454958	-1.5243025890
H	1.1889438313	-3.1647869165	-1.5336685576
H	-1.2232035039	-3.0477920149	-0.8682653259
H	-2.1583311279	-0.8429900487	-0.2232106412
N	-0.3947248602	0.1775653062	-0.5110828113
N	0.9975441354	2.5321398625	-0.4785379151
Cu	-0.8619987069	2.0364302788	-0.0706513058

$[H_2OCu(bpy)]^+$

	X	Y	Z
C	1.8754579967	1.3741308056	-0.9364481395
C	3.2517580815	1.3431899331	-1.1177109566
C	3.9687345118	2.5266898727	-1.0886698785
C	3.2948093309	3.7166889868	-0.8785263742
C	1.9232874558	3.6699139669	-0.7067637040
C	1.0353593914	0.1516353663	-0.9505567896
C	1.5606745886	-1.1201522746	-1.1360637095
C	0.7122479585	-2.2136378180	-1.1338731253
C	-0.6436710983	-2.0131322983	-0.9451331897
C	-1.0941031145	-0.7176777532	-0.7664183283
H	3.7680753582	0.4085743513	-1.2809252627
H	5.0422545334	2.5160631867	-1.2287164786
H	3.8132304833	4.6652799446	-0.8469538546
H	1.3572744649	4.5777060027	-0.5392830896
H	2.6211296673	-1.2664515532	-1.2803564680
H	1.1093409659	-3.2105714304	-1.2774873437
H	-1.3439295554	-2.8372164219	-0.9347742429
H	-2.1471759784	-0.5160897183	-0.6143347412

N	-0.2820274907	0.3380801558	-0.7689487802
N	1.2284420531	2.5336538212	-0.7347019619
Cu	-0.7519860625	2.2816737250	-0.5189523248
O	-2.3578038186	3.3440816716	-0.1885475756
H	-2.3906309291	4.3012458262	-0.2491054719
H	-3.2514533439	3.0188488716	-0.3168781892

$[N_2Cu(bpy)]^+$

	X	Y	Z
C	1.6163821603	1.3416119034	-0.9012653552
C	2.9867643407	1.4775303802	-1.0667875578
C	3.5555500046	2.7389889081	-1.0097277489
C	2.7437496969	3.8374739675	-0.7885783821
C	1.3857145021	3.6272925672	-0.6328782953
C	0.9200012570	0.0337977087	-0.9474465145
C	1.5780316306	-1.1697530859	-1.1540814626
C	0.8474784818	-2.3460031445	-1.1834145878
C	-0.5239180618	-2.2952501421	-1.0058825812
C	-1.1128019835	-1.0603446028	-0.8041601867
H	3.6125034354	0.6141064380	-1.2396519758
H	4.6239837407	2.8590667468	-1.1373613280
H	3.1458217103	4.8399682630	-0.7364780958
H	0.7111964882	4.4560304120	-0.4581216485
H	2.6490847348	-1.1993259760	-1.2914394592
H	1.3485275977	-3.2923062741	-1.3438347017
H	-1.1322084002	-3.1891902856	-1.0217895176
H	-2.1822372219	-0.9710099526	-0.6604393552
N	-0.4124261404	0.0728705229	-0.7752616539
N	0.8357120267	2.4147403960	-0.6873468716
Cu	-1.0924988701	1.9301537815	-0.4922476633
N	-2.6928007240	2.7693771776	-0.1989530471
N	-3.6499752159	3.2710489908	-0.0235158501

$[Ag(bpy)]^+$

	X	Y	Z
C	1.6525959228	1.4269141676	-0.8338328236
C	3.0318849517	1.4484924178	-1.0121667403
C	3.7063633604	2.6566120833	-0.9967855284
C	2.9924117300	3.8249744321	-0.7993539160
C	1.6266355995	3.7278035062	-0.6083282151
C	0.8912351100	0.1454614872	-0.8644511100
C	1.4614504086	-1.0191425835	-1.3676286745

C	0.7354089092	-2.1972038054	-1.3592793383
C	-0.5506292234	-2.1933837903	-0.8497381110
C	-1.0624262410	-0.9954381276	-0.3869218221
H	3.5857699088	0.5306702758	-1.1426051088
H	4.7802017882	2.6806049633	-1.1331397661
H	3.4755717606	4.7923988577	-0.7836321566
H	1.0287443946	4.6151351125	-0.4402865846
H	2.4580437031	-1.0108248854	-1.7836339184
H	1.1722091850	-3.1066933688	-1.7521456441
H	-1.1537221627	-3.0904977323	-0.8170120851
H	-2.0687814677	-0.9423872386	0.0100494184
N	-0.3655813667	0.1396165131	-0.3973174524
N	0.9766839714	2.5653839051	-0.6221777319
Ag	-1.1701712324	2.2125377104	-0.0284899712

$[H_2OAg(bpy)]^+$

	X	Y	Z
C	1.8947092682	1.3695633852	-0.9575192466
C	3.2809287191	1.2768365944	-1.0253076557
C	4.0416836009	2.4315817417	-1.0642537706
C	3.4034687064	3.6586580110	-1.0317468871
C	2.0230932890	3.6715790852	-0.9465401080
C	1.0340911551	0.1570730105	-0.9274077590
C	1.5369710459	-1.1006308405	-1.2442690470
C	0.7044863147	-2.2038231902	-1.1861913210
C	-0.6168892004	-2.0300378840	-0.8144451648
C	-1.0495667897	-0.7474125296	-0.5316269603
H	3.7712930502	0.3144537613	-1.0289776415
H	5.1215065420	2.3700535639	-1.1144918053
H	3.9552058595	4.5883304117	-1.0633958843
H	1.4832961251	4.6100278804	-0.9089214853
H	2.5648083284	-1.2229734289	-1.5528209414
H	1.0856603466	-3.1866866723	-1.4331339063
H	-1.3043085397	-2.8624949743	-0.7498039673
H	-2.0779619060	-0.5649970864	-0.2443160361
N	-0.2515433893	0.3167289681	-0.5887882577
N	1.2882107151	2.5622072235	-0.9081065722
Ag	-0.9434698259	2.4798705334	-0.4530439582
O	-2.7013682930	3.7911392564	-0.0668762875
H	-2.8168887217	4.6340290241	-0.5115242507
H	-3.5810592404	3.4408092051	0.0907467638

$[N_2Ag(bpy)]^+$

	X	Y	Z
C	1.6117506407	1.3560249836	-0.8988312492
C	2.9868258016	1.4684865162	-1.0718290297
C	3.5832532670	2.7159702963	-1.0241010633
C	2.7957929629	3.8321021009	-0.8051564757
C	1.4351745270	3.645 8478944	-0.6459799770
C	0.9185737242	0.0399331591	-0.9374580244
C	1.6143175237	-1.1536558789	-1.0954074024
C	0.9212391694	-2.3506358115	-1.1298692337
C	-0.4565427085	-2.3360136592	-1.0052166194
C	-1.0813475322	-1.1130518513	-0.8463415016
H	3.5979301528	0.5958923334	-1.2471197622
H	4.6534359587	2.8113951027	-1.1578899366
H	3.2173494404	4.8269250490	-0.7588822775
H	0.7792586141	4.4904408782	-0.4744602431
H	2.6899308520	-1.1615360566	-1.1878246462
H	1.4558843465	-3.2841446736	-1.2522984342
H	-1.0405172745	-3.2459770967	-1.0276252414
H	-2.1577627927	-1.0531382449	-0.7424716241
N	-0.4156780923	0.0399338424	-0.8124028088
N	0.8594201358	2.4456507826	-0.6917792660
Ag	-1.3488760752	2.0636666685	-0.4948487915
N	-3.2157508084	3.0280010772	-0.2004754995
N	-4.1760270231	3.5234868683	-0.0523947325

$[Au(bpy)]^{+}$

	X	Y	Z
C	1.6574939171	1.4245516852	-0.8363873340
C	3.0351066691	1.4520710880	-1.0201298328
C	3.7046019571	2.6631687721	-1.0019221416
C	2.9880943494	3.8287414826	-0.7964823714
C	1.6231113233	3.7312280418	-0.6011932701
C	0.8961042748	0.1423624565	-0.8650477865
C	1.4618030427	-1.0253542191	-1.3637415382
C	0.7292447588	-2.1996240573	-1.3552149826
C	-0.5583232963	-2.1899365649	-0.8492825145
C	-1.0695061299	-0.9918446596	-0.3869002109
H	3.5910258627	0.5363572121	-1.1563973027
H	4.7777725257	2.6914684800	-1.1421826059
H	3.4685373996	4.7975156811	-0.7788816214
H	1.0189724918	4.6120757528	-0.4286929500
H	2.4595828429	-1.0216684118	-1.7768607062
H	1.1626243053	-3.1116346092	-1.7458243439

H	-1.1652126335	-3.0845376828	-0.8170284007
H	-2.0741060643	-0.9291269391	0.0099696195
N	-0.3600471376	0.1355268731	-0.4001494244
N	0.9846861829	2.5624285707	-0.6202713278
Au	-1.1276676316	2.1872649481	-0.0362562338

$[H_2OAu(bpy)]^+$

	X	Y	Z
C	1.9076172942	1.4119483897	-1.0056280884
C	3.2736410950	1.3197401158	-0.7563779393
C	4.0413126686	2.4704427580	-0.8222401981
C	3.4261053943	3.6701629348	-1.1336320856
C	2.0559112765	3.6688302339	-1.3485719010
C	1.0488831376	0.2043162908	-0.9763039239
C	1.5783540316	-1.0453134255	-1.2788691432
C	0.7786479065	-2.1708405755	-1.2509914245
C	-0.5584052962	-2.0326392049	-0.9190652601
C	-1.0372140654	-0.7719701615	-0.6393624813
H	3.7303178578	0.3768145927	-0.4881283564
H	5.1052453617	2.4280218365	-0.6259520061
H	3.9885817025	4.5918562952	-1.2022565618
H	1.5333495227	4.5891188332	-1.5865660732
H	2.6173997234	-1.1224255369	-1.5649165786
H	1.1924781603	-3.1412932438	-1.4941841660
H	-1.2293132730	-2.8795630479	-0.8802925802
H	-2.0731475112	-0.6141899344	-0.3770522334
N	-0.2588181070	0.3219807332	-0.6696144250
N	1.3141813863	2.5712272876	-1.2853233097
Au	-1.1455671390	2.1163996301	-0.3373562023
O	-2.1564328097	3.9119523928	0.0537618737
H	-2.7512969194	3.8712879181	0.8099281208
H	-2.6674048180	4.2490475383	-0.6897696961

$[N_2Au(bpy)]^+$

	X	Y	Z
C	1.5980063015	1.3470493136	-0.9021838056
C	2.9698449726	1.4717327362	-1.0802852331
C	3.5645144119	2.7188571516	-1.0371576265
C	2.7752085563	3.8339648035	-0.8153874375
C	1.4186723854	3.6510558945	-0.6485416140
C	0.9115043023	0.0335670030	-0.9384854417
C	1.5967331765	-1.1658615265	-1.0942424081

C	0.8798940577	-2.3502683912	-1.1220703253
C	-0.4972880087	-2.3106267460	-0.9936945847
C	-1.1038340971	-1.0753474082	-0.8377129076
H	3.5769833804	0.5968689697	-1.2574521288
H	4.6337342327	2.8164428351	-1.1765764948
H	3.1921561552	4.8305966575	-0.7719898059
H	0.7600801194	4.4901037680	-0.4741048007
H	2.6723303583	-1.1919213039	-1.1890407583
H	1.3964973571	-3.2941280345	-1.2421812304
H	-1.0945156655	-3.2122802784	-1.0113149191
H	-2.1791289167	-0.9935119420	-0.7309720738
N	-0.4155040848	0.0591108447	-0.8112674237
N	0.8446400637	2.4414005498	-0.6914726487
Au	-1.2414719678	2.3035283482	-0.4547286428
N	-3.1124598884	2.8182151691	-0.1693061936
N	-4.1675044120	3.0637778261	-0.0149380354

$[Ag(phen)]^{+}$

	X	Y	Z
C	-3.1046575186	-6.6160060046	-0.0042996648
C	-1.7364565523	-6.6703347030	-0.0052496996
C	-0.9889124535	-5.4805120830	-0.0037390483
C	-1.6922567409	-4.2585379288	-0.0013003934
C	-3.7203440720	-5.3629875073	-0.0017808653
C	0.4361890752	-5.4928891631	-0.0046382419
C	-0.9413650557	-3.0207641710	0.0001564646
C	0.4673027390	-3.0797896921	-0.0009309082
C	1.1368335166	-4.3377827578	-0.0032808041
C	1.1772403804	-1.8672568013	0.0003575923
H	2.2607544748	-1.8886995234	-0.0004508735
C	0.4969290750	-0.6788901724	0.0026079697
C	-0.8987907150	-0.7117156358	0.0036520925
H	0.9442788929	-6.4494897949	-0.0064478850
H	-3.7108119466	-7.5116976360	-0.0053940385
H	-1.2169579281	-7.6214324461	-0.0071585695
H	-4.8011972601	-5.2872041001	-0.0009023197
H	2.2199437826	-4.3460315166	-0.0039566740
H	1.0112534585	0.2724944326	0.0036288275
H	-1.4655208609	0.2117136591	0.0055376677
N	-1.5907378810	-1.8360952532	0.0024833055
N	-3.0428999082	-4.2300352770	-0.0003516604
Ag	-3.8259653422	-2.1115658941	0.0042491564

$[H_2OAg(phen)]^+$

	X	Y	Z
C	-4.6164725612	-5.3538543055	0.0071096008
C	-3.2538785327	-5.4952523405	-0.0088998920
C	-2.4364602024	-4.3537538983	-0.0096710720
C	-3.0674444682	-3.0935082091	0.0056579862
C	-5.1534708805	-4.0648182401	0.0217243039
C	-1.0134541660	-4.4433068490	-0.0244213999
C	-2.2512420508	-1.9017591327	0.0069205927|
C	-0.8482099609	-2.0340977185	-0.0067263343
C	-0.2500032991	-3.3283989145	-0.0228873357
C	-0.0796879648	-0.8590676577	-0.0028951711
H	1.0016510023	-0.9306072721	-0.0129367112
C	-0.7044755987	0.3601133594	0.0142323676
C	-2.1004913439	0.3941487650	0.0266740183
H	-0.5578817363	-5.4260512898	-0.0362566184
H	-5.2761507969	-6.2109780712	0.0089571444
H	-2.7960644723	-6.4774730922	-0.0204494984
H	-6.2277444745	-3.9235805873	0.0353327082
H	0.8309990020	-3.3978916038	-0.0333742777
H	-0.1440842071	1.2851975498	0.0185489077
H	-2.6209185417	1.3445361238	0.0411073650
N	-2.8485553198	-0.6932070601	0.0225756577
N	-4.4103591314	-2.9739156522	0.0206430677
Ag	-5.1266617961	-0.8122271557	0.0444786713
O	-6.9518298874	0.4651593199	0.1184970275

$[N_2Ag(phen)]^+$

	X	Y	Z
C	-2.9274271129	-6.7930895685	-0.0050217298
C	-1.5571051667	-6.7999951250	-0.0052117580
C	-0.8546227201	-5.5838222990	-0.0037125345
C	-1.6066853196	-4.3929250880	-0.0020144814
C	-3.5902451230	-5.5641693652	-0.0033237322
C	0.5702798407	-5.5300267572	-0.0038872466
C	-0.9153185142	-3.1268407986	-0.0004818398
C	0.4932094780	-3.1158935876	-0.0007503130
C	1.2181195993	-4.3437925084	-0.0024719901
C	1.1366926491	-1.8675315504	0.0007186207
H	2.2196895631	-1.8272063738	0.0005270786
C	0.3901142299	-0.7184524161	0.0023441977
C	-1.0020770973	-0.8250252671	0.0025344076
H	1.1225729166	-6.4618746556	-0.0052046368

H	-3.4996403875	-7.7108503141	-0.0061831921
H	-1.0056065211	-7.7329352889	-0.0065496389
H	-4.6730719970	-5.5279339888	-0.0031503911
H	2.3006261829	-4.3046718318	-0.0026280341
H	0.8530127423	0.2590080235	0.0034833206
H	-1.6177428662	0.0664894338	0.0038198807
N	-1.6336877116	-1.9847582061	0.0011961619
N	-2.9558856982	-4.4059796087	-0.0018103639
Ag	-3.8591311866	-2.3423442863	0.0014629824
N	-5.7237856552	-1.3207227946	0.0031591766
N	-6.6798233446	-0.7958345076	0.0039703454

$[Au(Phen)]^{+}$

	X	Y	Z
C	-3.8217155493	-6.1146933588	-0.0043636057
C	-2.4528790581	-6.1738660321	-0.0050338003
C	-1.7001758370	-4.9878496526	-0.0036414270
C	-2.3986755948	-3.7641348783	-0.0013597977
C	-4.4373162066	-4.8625724643	-0.0019444306
C	-0.2747472281	-5.0005952078	-0.0045373477
C	-1.6465546781	-2.5275991986	0.0000055407
C	-0.2387962956	-2.5863013227	-0.0009372766
C	0.4274969828	-3.8464625923	-0.0032353005
C	0.4688715447	-1.3728657942	0.0003761847
H	1.5523707090	-1.3913393900	-0.0004947529
C	-0.2129671652	-0.1844836129	0.0024474442
C	-1.6083744567	-0.2132541210	0.0036275806
H	0.2325793871	-5.9575727744	-0.0062396363
H	-4.4297629297	-7.0090959049	-0.0057440885
H	-1.9387851856	-7.1277956660	-0.0069807990
H	-5.5162653627	-4.7771756847	-0.0015247019
H	1.5105668721	-3.8572264083	-0.0038678495
H	0.3021441855	0.7664983973	0.0032330313
H	-2.1801697566	0.7058067798	0.0051315724
N	-3.7474760243	-3.7365268410	-0.0001899528
N	-2.2917435211	-1.3428795906	0.0026071778
Au	-4.4971574917	-1.6523342816	0.0054576651

$[H_2OAu(phen)]^{+}$

	X	Y	Z
C	-3.9295162018	-5.9229875418	-0.0327478645
C	-2.5687822861	-6.0749355964	-0.0188729299

C	-1.7424279254	-4.9386502568	-0.0066455599
C	-2.3707463748	-3.6752126074	-0.0092652580
C	-4.4544120042	-4.6248207895	-0.0341973079
C	-0.3219926038	-5.0409742322	0.0079022277
C	-1.5475877359	-2.4875587332	0.0029619998
C	-0.1430385677	-2.6321487110	0.0173695474
C	0.4462573083	-3.9306123562	0.0194881647
C	0.6525084855	-1.4780734276	0.0292454966
H	1.7313938306	-1.5787927106	0.0402151427
C	0.0609950135	-0.2423498926	0.0268072186
C	-1.3262857047	-0.1694248088	0.0122821792
H	0.1284594277	-6.0262580638	0.0094363952
H	-4.5942708355	-6.7765400963	-0.0424507566
H	-2.1169504584	-7.0599650276	-0.0172237217
H	-5.5283958141	-4.4694404177	-0.0451537093
H	1.5268766897	-4.0020069869	0.0305228168
H	0.6404400010	0.6703439228	0.0356983996
H	-1.8276935517	0.7874362992	0.0098015159
N	-3.7048584968	-3.5456625282	-0.0228109260
N	-2.1056133632	-1.2481049241	0.0006752144
Au	-4.1192255663	-0.9505835320	-0.0215703197
O	-6.1748091872	-0.4884973408	-0.0477735649
H	-6.4407533888	0.0358777132	-0.8105648117
H	-6.4719959401	-0.0122254436	0.7348013416

$[N_2Au(phen)]^+$

	X	Y	Z
C	-3.7644459589	-6.2115669384	-0.0058824215
C	-2.3947366517	-6.2506061575	-0.0046221093
C	-1.6659037533	-5.0490289738	-0.0031903701
C	-2.4008950643	-3.8481278978	-0.0031690251
C	-4.4017685211	-4.9652798960	-0.0056939370
C	-0.2409209862	-5.0144104185	-0.0018109727
C	-1.6950574573	-2.5948027564	-0.0017625571
C	-0.2865266912	-2.5975552456	-0.0004243946
C	0.4212618417	-3.8358466238	-0.0004801583
C	0.3773742265	-1.3618075258	0.0009119393
H	1.4608401831	-1.3401319059	0.0019331318
C	-0.3484154785	-0.1983536330	0.0008921947
C	-1.7374019310	-0.2736503752	-0.0004676903
H	0.3015736477	-5.9520861618	-0.0018450091
H	-4.3553893465	-7.1176768474	-0.0069902025
H	-1.8646326786	-7.1957877979	-0.0046982414

H	-5.4844845818	-4.9041836835	-0.0066252048
H	1.5039325107	-3.8084764025	0.0005735424
H	0.1294416419	0.7715219018	0.0018957332
H	-2.3389512756	0.6245363311	-0.0005226207
N	-3.7423952430	-3.8265901522	-0.0043834380
N	-2.3906252932	-1.4314835030	-0.0017300661
Au	-4.4677116050	-1.4372964194	-0.0037939963
N	-6.3668487900	-0.9380331552	-0.0052481986
N	-7.4338241444	-0.6985335023	-0.0060449177

$[Cu(phen)]^+$

	X	Y	Z
C	-3.3435375290	-5.7496854575	-0.0028324001
C	-1.9752259117	-5.8233192761	-0.0041648019
C	-1.2114804621	-4.6432564511	-0.0028532919
C	-1.9024962610	-3.4187750802	-0.0000351755
C	-3.9501199172	-4.4919225956	-0.0001973146
C	0.2146380142	-4.6558664096	-0.0043539676
C	-1.1501242834	-2.1858054131	0.0014297151
C	0.2548860475	-2.2395005888	-0.0002217086
C	0.9188683181	-3.5015247388	-0.0031317016
C	0.9541679985	-1.0201752465	0.0010860276
H	2.0378421798	-1.0287993431	-0.0001918308
C	0.2620527362	0.1626087531	0.0038827761
C	-1.1338799237	0.1260038129	0.0055136929
H	0.7229831371	-5.6123458652	-0.0066140015
H	-3.9587792666	-6.6391043038	-0.0039320528
H	-1.4713418258	-6.7827574037	-0.0064578594
H	-5.0292951913	-4.4013903245	0.0007435602
H	2.0019299561	-3.5155164371	-0.0043371688
H	0.7710701116	1.1168049592	0.0049417880
H	-1.7088437059	1.0437151847	0.0078416697
N	-3.2579819266	-3.3664377203	0.0012751351
N	-1.8170768539	-1.0049812225	0.0043878003
Cu	-3.7358810110	-1.4539783023	0.0061340600

$[H_2OCu(phen)]^+$

	X	Y	Z
C	-3.3856962568	-5.6306575147	-0.0105350016
C	-2.0222202727	-5.7744063809	0.0042649997
C	-1.2059657681	-4.6314139751	0.0067127417
C	-1.8453361603	-3.3800603957	-0.0055251035

C	-3.9302908111	-4.3437343841	-0.0219578275
C	0.2196194629	-4.6943396931	0.0199208422
C	-1.0532280484	-2.1815726293	-0.0060979242
C	0.3484954812	-2.2786773802	0.0057703959
C	0.9655148954	-3.5654105972	0.0194656913
C	1.0801241792	-1.0797874627	0.0024065527
H	2.1632675858	-1.1134323688	0.0111296345
C	0.4134295144	0.1182811546	-0.0126524316
C	-0.9837653507	0.1152679560	-0.0235809275
H	0.6942363261	-5.6680510841	0.0297423610
H	-4.0438223495	-6.4889777256	-0.0137657283
H	-1.5668637505	-6.7577508479	0.0134474202
H	-5.0047709120	-4.2060508476	-0.0345566840
H	2.0473615948	-3.6199532332	0.0288537579
H	0.9449605434	1.0602250068	-0.0165356640
H	-1.5315998394	1.0495915514	-0.0363767080
N	-3.1898889863	-3.2497120979	-0.0189641946
N	-1.7002059640	-0.9951254680	-0.0199446685
Cu	-3.6886024793	-1.2852657460	-0.0334061938
O	-5.3513789136	-0.2529813922	-0.0844356858
H	-5.4002697177	0.6891739118	0.0915419767|
H	-6.2151169927	-0.6240509162	0.1084925991

$[N_2Cu(phen)]^+$

	X	Y	Z
C	-3.2742779992	-5.8626919114	-0.0021617713
C	-1.9032924597	-5.9069038407	-0.0059144237
C	-1.1697077765	-4.7083198430	-0.0041582526
C	-1.8988800911	-3.5087754793	0.0014095930
C	-3.9137248119	-4.6204267724	0.0034204423
C	0.2568198845	-4.6621070729	-0.0077981483
C	-1.2016090411	-2.2555040616	0.0034101978
C	0.2021916088	-2.2426731453	-0.0002833719
C	0.9150095797	-3.4791150711	-0.0059339301
C	0.8339412916	-0.9874892823	0.0018336141
H	1.9162887860	-0.9326697767	-0.0008767949
C	0.0734491106	0.1541046158	0.0073118885
C	-1.3192079719	0.0426061787	0.0106949604
H	0.8048918933	-5.5964085409	-0.0121073813
H	-3.8677580920	-6.7668037262	-0.0034367422
H	-1.3792089207	-6.8554812343	-0.0102490283
H	-4.9950366464	-4.5580176530	0.0063216168
H	1.9978526613	-3.4519432433	-0.0087112732

H	0.5287283439	1.1350958645	0.0090720588
H	-1.9421759676	0.9286243123	0.0150490408
N	-3.2503811425	-3.4771889992	0.0050733132
N	-1.9409878509	-1.1238774797	0.0088301033
Cu	-3.8952314937	-1.5769847888	0.0126669028
N	-5.4989577244	-0.6861875121	0.0200355891
N	-6.4564303204	-0.1555257270	0.0244306871

H_2O

	X	Y	Z
O	-0.0127595829	-0.4993376679	0.0000000000
H	0.9443155624	-0.4566627288	0.0000000000
H	-0.2920105695	0.4170859768	0.0000000000

N_2

	X	Y	Z
N	-4.3943423920	0.1470588200	0.0000000000
N	-5.4844223880	0.1470588200	0.0000000000